

MANTLE-DERIVED BASANITE FEATURES
AND THEIR INCLUSIONS FROM
THE NORTH RIM OF THE GRAND CANYON
NATIONAL MONUMENT, ARIZONA

A Thesis
Submitted to
the Temple University Graduate Board

in Partial Fulfillment
of the Requirements for the Degree
Master of Arts

by
Linus J. Farias

June, 1989


DR. GENE C. ULMER
Thesis Advisor

ABSTRACT

Over one hundred and fifty basanite features are located in a 12.1 square kilometer (4.73 square mile) area on the north rim of the Grand Canyon National Monument, at the southern edge of the Toroweap Valley. Thirty - six of these were analyzed to determine their origin. The features, previously described as "Pressure blisters" (Hamblin and Best, 1970), are believed to be direct mantle orifices that have erupted under an ash or lava cover. Green and red colored peridotite xenoliths of varying dimensions are found enclosed within these features on the Toroweap Valley as well as on the adjacent cinder cone Vulcan's Throne. The unique red coloring, observed primarily in forsteritic olivine (FO_{90-92}), is believed to be a result of precipitation of a ferric rich phase within individual olivine grains.

Results obtained from a theoretical single-pyroxene geothermobarometer (Mercier, 1980) suggest pressures of at least 15 kilobars and temperatures of at least 940°C, corresponding to a depth of origin of at least 52 kilometers for the Toroweap Valley features. A genetic model developed suggests that the basanite lava carrying green colored olivine originated from a magma chamber at least 52 kilometers below the ground surface, transected a shallower magma chamber in which red colored xenoliths are suspended and punctured the crust in the Toroweap Valley.

ACKNOWLEDGEMENTS

I offer this thesis to my creator who made this project possible.

I am indebted to my thesis advisor Dr. Gene Ulmer for being a professional and personal ally in good times and bad. Thanks also go to my thesis committee members, Dr. David Grandstaff and Dr. George Myer for their guidance and support throughout this project. Special thanks go to Dr. Peter Goodwin for his "fatherly" support when I was alien to Temple University and its ways and for helping me tie this up!

I am grateful to the United States Department of the Interior (National Park Service, Grand Canyon National Park, Arizona) and especially to Mr. Douglas Brown for permitting us to work in the Grand Canyon National Monument. I thank Ms. Renee J. Beymer, the park ranger during our visit, for all her help especially when we were stranded.

I thank Mr. Lee Eminhizer (Pennsylvania State University) for his guidance during electron microprobe analysis and Mr. Steven Sylvester (Franklin and Marshall College) for educating me in the X-ray fluorescence technique. Mr. Ben Hanson is thanked for permitting me free use of his Vulcan's Throne samples and data.

Mrs. Miranda Blau and Mrs. Wilhelmenia Simpson are sincerely thanked for always "being there". I will always treasure their listening ears! Thanks also to Lt. John Sego for helping out with my photography.

My colleagues at Temple are thanked especially Mr. Jianhua Wang and Mr. Youngdo Park. Ms. Pranoti Asher (University of Connecticut) is thanked for her encouraging and enlightening input especially with the X-ray fluorescence analysis. I'm also sincerely grateful to my family and friends here and in India for tolerating me during the last three years.

I finally thank my wife and moral support, Diana, for her love and forbearance ever since I met her.

TABLE OF CONTENTS

iv

TITLE.....i
ABSTRACT.....ii
ACKNOWLEDGMENTS.....iii
TABLE OF CONTENTS.....iv
LIST OF FIGURES.....vii
LIST OF TABLES.....x
LIST OF APPENDICES.....xi

INTROOUCION.....1

DESCRIPTION AND GENESIS OF BASANITE FEATURES.....5

 Introduction.....5

 Regional History.....5

 Source of Information.....8

 Geomorphology of the study area.....8

Geomorphology and Structure of the features.....9

Xenolithic Inclusions.....17

 Settling Velocity calculation.....19

 Assumptions.....20

 Method of calculation.....21

 Discussion of results.....25

TABLE OF CONTENTS (contd)

v

Chemistry of basanite features.....	30
Introduction.....	30
X-ray fluorescence method.....	31
Discussion of results.....	34
Hypothesis of origin.....	44
Summary of results.....	47
ANALYSIS OF PERIDOTITE XENOLITHS.....	50
Petrography.....	50
Introduction.....	50
Sample Preparation.....	53
Reheating of Xenoliths.....	59
Method developed to reheat xenoliths....	60
Discussion of results.....	63
Red colored xenoliths in thin section.....	63
Introduction.....	63
Alteration of Olivine.....	69
Spinel and their alteration.....	74
Summary and Discussion.....	78
Geothermometry and Geobarometry.....	80
Introduction.....	80
Method of analysis.....	80
Electron microprobe sample preparation.....	81

TABLE OF CONTENTS (contd)

vi

Electron Microprobe analysis.....	82
Theory and limits of the thermobarometer.....	83
Results.....	85
Spinel-facies stability results.....	86
Garnet-facies stability results.....	90
Discussion.....	93
CONCLUSIONS.....	97
REFERENCES.....	100
APPENDICES.....	107

LIST OF FIGURES

vii

<u>FIGURE</u>	<u>SUBJECT</u>	<u>PAGE</u>
1	Topographic map showing field area.....	2
2	Aerial view of the Toroweap Valley.....	3
3	Index map of major faults in field area.	7
4	Location of analyzed features.....	10
5	Ridge-shaped feature.....	12
6	Beehive-shaped feature.....	13
7	Typical polygonal cracks.....	14
8	Spatter-cone feature.....	16
9	Peridotite xenoliths in basanite features.....	18
10	Viscosity <u>vs</u> Temperature for basalt lava.....	23
11	Viscosity <u>vs</u> Distance travelled for xenoliths in a basanite lava.....	27
12	Schematic representation of X-ray fluorescence spectrophotometer.....	33
13	TiO ₂ vs MgO/(FeO + 0.9Fe ₂ O ₃).....	37
14	MgO vs MgO/(FeO + 0.9Fe ₂ O ₃).....	39
15	CaO vs MgO/(FeO + 0.9Fe ₂ O ₃).....	40
16	Map of localized basanite flows.....	42

LIST OF FIGURES (CONTD)

viii

<u>FIGURE</u>	<u>SUBJECT</u>	<u>PAGE</u>
17	Cartoon representation of Toroweap feature evolution.....	43
18	Ternary phase diagram showing crystallization sequence of lavas.....	45
19	TYPE G* xenolith in hand sample and thin section.....	55
20	TYPE C xenolith in hand sample and thin section.....	58
21	Schematic diagram of reheating furnace..	61
22	Green xenolith heated in air.....	64
23	Green xenolith heated in CO ₂	65
24	Hand samples of red and green colored xenoliths.....	67
25	Hand sample of TYPE G* xenolith.....	68
26	Photomicrograph of ferric-rich strands in red-colored olivine.....	71
27	Photomicrograph of secondary ferric-rich strands in red colored olivine.....	72
28	Photomicrograph of spinel in fractured zone.....	75
29	Photomicrograph of necklace-like growth around a spinel grain.....	77

LIST OF FIGURES (CONTD)

ix

<u>FIGURE</u>	<u>SUBJECT</u>	<u>PAGE</u>
30	Pressure-temperature-depth (spinel facies).....	88
31	Pressure-temperature-depth (garnet facies).....	92

LIST OF TABLES

x

<u>Table</u>	<u>Subject</u>	<u>Page</u>
1	Results of Settling Velocity Calculation.....	26
2	Results of X-ray Fluorescence Analysis....	35
3	Results of Geothermobarometry..... (Spinel Facies)	87
4	Results of Geothermobarometry..... (Garnet Facies)	91

LIST OF APPENDICES

xi

I.	BASIC program for Settling Velocity Calculation.....	107
II.	BASIC program for Thermobarometric Calculation (Spinel-stability facies).....	108
III.	BASIC program for Thermobarometric Calculation (Garnet-stability facies).....	110

INTRODUCTION

The Grand Canyon is one of the most exotic natural wonders of the world not only aesthetically, but also geologically. An infinitesimal but very meaningful part of this National Monument includes recent lava flows in the Toroweap Valley, which is the focus of this study (Figure 1).

The study area is located on the north rim of the Grand Canyon at an elevation of about 1555 meters (4500 feet) above mean sea level. It is a 12.1 square kilometer (4.73 mi²) area (3.5 km X 3.42 km) lying between latitudes 36° 12' 45" N and 36° 14' 36" N, and longitudes 113° 05' 07" W and 113° 07' 30" W. Field work and sampling was undertaken in a 6 square kilometer (2.35 mi²) area within the Valley (Figure 2).

Unique to the Toroweap Valley flows is an irregular scatter of igneous extrusive features trending roughly northwest - southeast in a localized area just west of Vulcan's Throne. The features vary in dimensions too -- 1 to 15 meters (3 - 50 feet) in horizontal extension to over 5 meters (16 feet) in vertical elevation. Traditionally viewed as pressure blisters (Hamblin and Best, 1970), these features vary widely in shape and size. Variable morphology suggests that the features are not simple pressure blisters. The presence of large (kilogram-size) peridotite xenoliths supports the idea that the

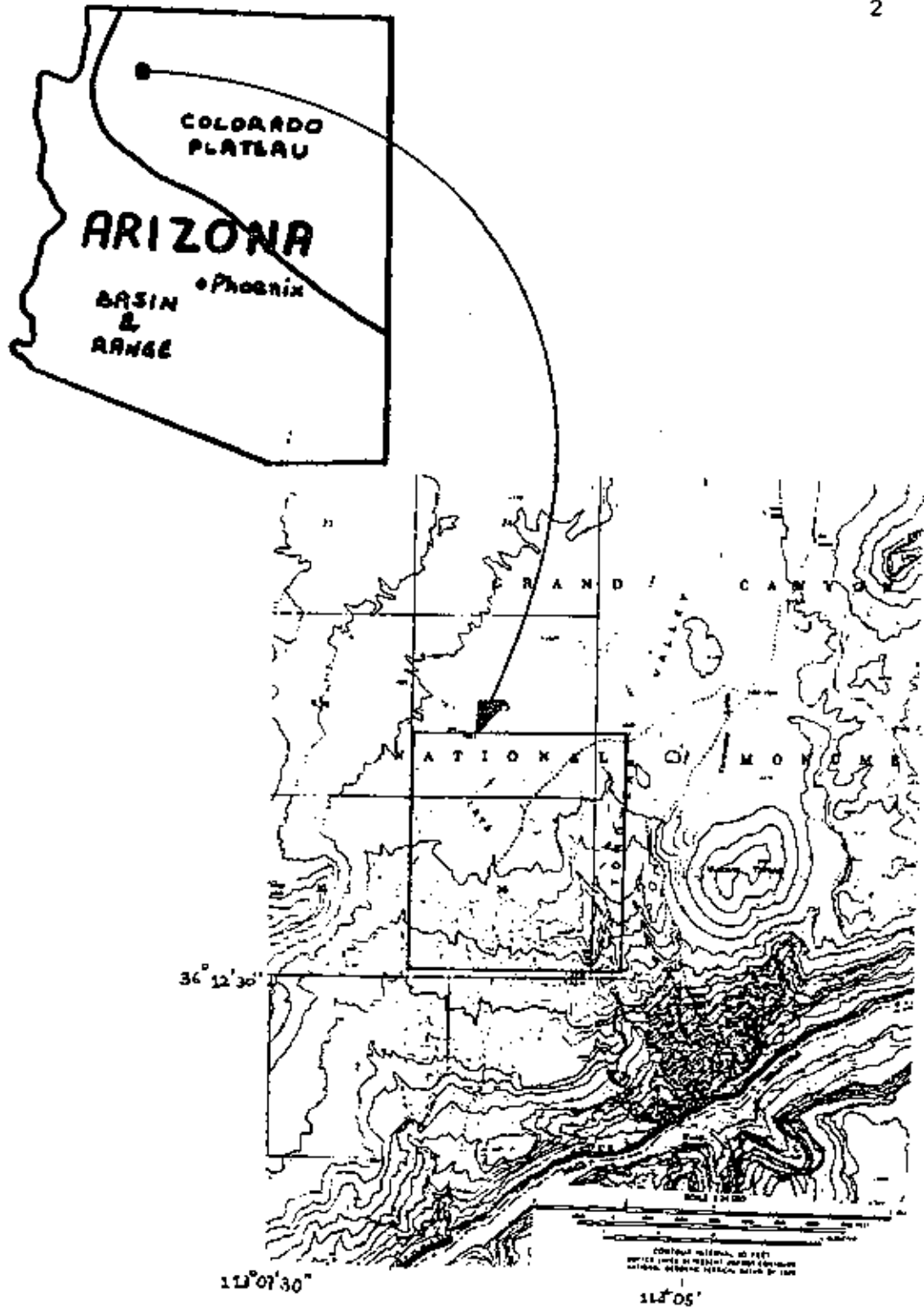


Figure 1. Topographic map of the southern Toroweap Valley (box encloses the study area)



Figure 2. Aerial photograph of the Toroweap Valley with the basanite features sitting on the flows (looking west from Vulcan's Throne)

features may be direct mantle orifices.

The purpose of this study is to determine the origin of the basanite features in the Toroweap Valley. The first section describes the area, the basanite features, and the relationship between the two. A geomorphic analysis describes vent characteristics of the features and (from chemical analysis), a model is developed suggesting an eruption mechanism for the Toroweap vent features and the adjacent alkali olivine basalt cinder cone, Vulcan's Throne.

The second section describes the xenoliths found in the features on the Valley. Results from a petrographic analysis of the xenoliths is compared with those of Best (1974). A theoretical single pyroxene geothermometer (Mercier, 1980), applied to pyroxenes from the different textural types of xenoliths, provides a means of estimating the minimum depths of crystallization of the silicate phase.

The final section summarizes the study and lists the conclusions that are drawn from them.

DESCRIPTION AND GENESIS OF BASANITE FEATURES

INTRODUCTION

The Toroweap basanite features are found scattered throughout the southern end of the Toroweap Valley, just west of the widely studied alkali olivine basalt cinder cone, Vulcan's Throne. The Toroweap Valley is a broad, flat valley, approximately 3.2 kms (2 miles) in width that lies in the tectonically active transition zone between the Basin and Range province and the Colorado Plateau. It is considered by some workers to be a part of the Basin and Range Province (Christiansen and Lipman, 1970, Brumbaugh, 1987), and by others to be a part of the Colorado Plateau (Hamblin and Best, 1970). For a general geology of the Grand Canyon area, the reader is referred to manuscripts by Hamblin and Best (1970) and Breed and Roat (1974).

Regional history

The western Grand Canyon area underwent extensive volcanism as a result of major fault movement during Pliocene and Pleistocene time. Evidence for this tectonism is seen in the major, roughly North-South

trending normal step-faults that transect the region (Figure 3). The associated lavas are generally basaltic in nature and are believed to be formed as a result of Basin and Range-type extensional tectonics over the past seven million years (Best and Brimhall, 1974 p.1685). Many series of flows have been named and described in the Toroweap Valley (Powell, 1875; Dutton, 1882; Koons, 1945; Hamblin and Best, 1970). The basanite flows in the Toroweap Valley originated from vents located high up on the Uinkaret Plateau, about 10 kilometers north of the canyon rim (Figure 2). They flowed south until they cascaded over the edge of the canyon. The youngest of these lava flows is manifest at the edge of the canyon as the spectacular "Frozen Lava Falls" that cascade over the rim of the canyon. The youngest lava, believed to be younger in age than the last Vulcan's Throne eruption (Hamblin and Best, 1970), is estimated as being ten to twenty thousand years old. Havisupai legend would suggest a catastrophic failure of a lava dam on the Colorado river as recently as 800 years ago (J.Riffe, verbal communication; 1978).

The ground surface in the field area is covered with cinders (presumably from regional volcanism), sage shrubs and tumbleweed, thus limiting the surface exposure of the individual flows.

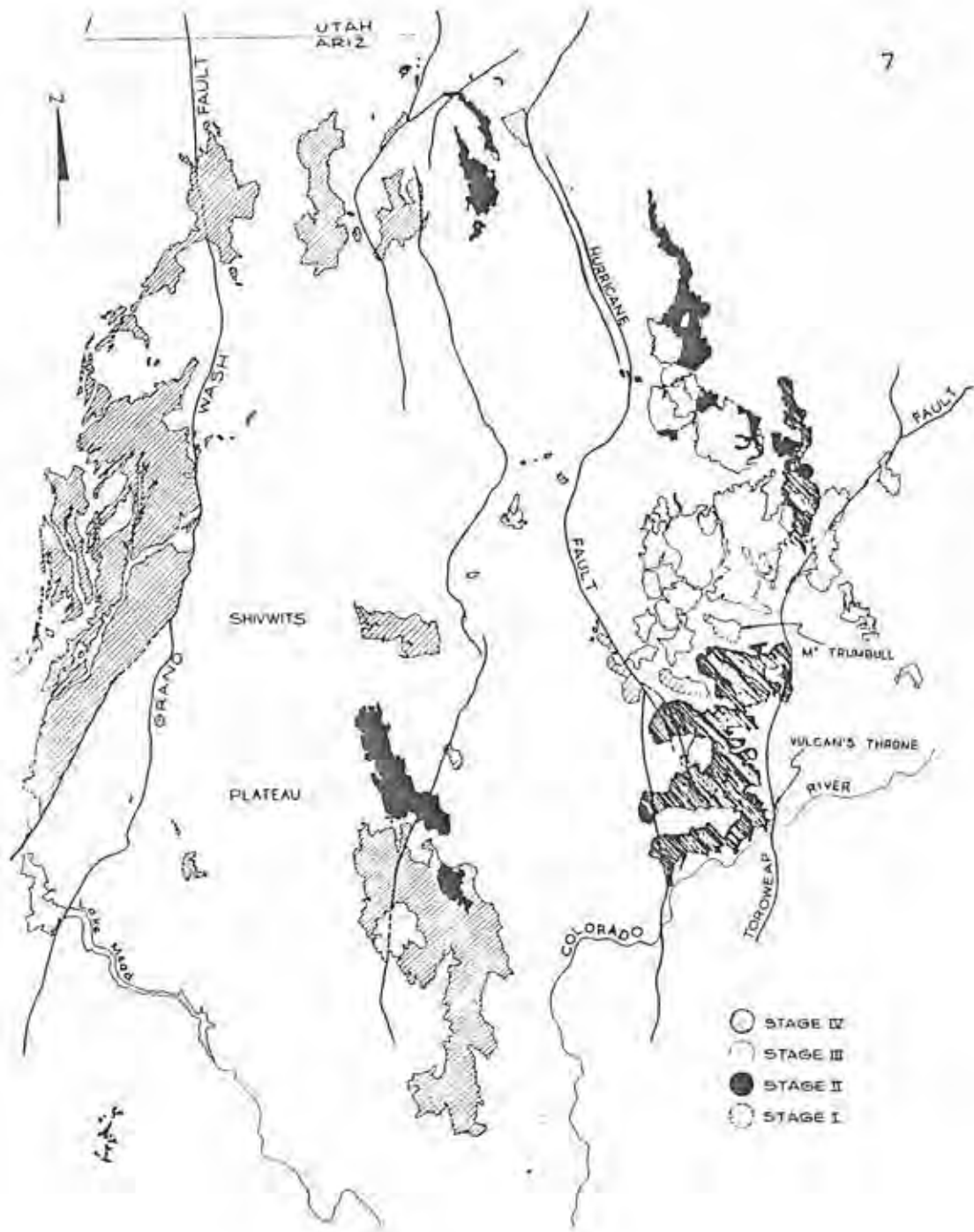


Figure 3. Index map of major faults and major basaltic flows in the Western Grand Canyon region (from Hamblin, 1974)

Sources of Information

A comprehensive geomorphic analysis of the Toroweap Valley was synthesized from field studies, topographic maps, high-angle and low-angle aerial photographs, and video coverage (G. C. Ulmer, pers. comm) from the ground. The high-angle aerial photographs, obtained from the United States Geological Survey (USGS) archives, in conjunction with topographic maps of the area, provided a spatial distribution grid for the features from within the field area as well as adjacent localities. Low-angle photographs were taken by the author and Dr. G. C. Ulmer. Video tape coverage was useful in providing a descriptive overview of the study area.

Geomorphology of the study area

The southwestern region of the United States, and specifically the Western Grand Canyon region currently has a very arid climate. The Toroweap Valley typically has a gentle slope of about 0.03428 or 1:29 gradient. It is transected by roughly north-south trending intermittent streams that turn toward the northwest at the northern end of the study area. Though intermittent and small, these streams have cut gullies in some areas as much as 6 meters (approx. 20 feet) below the mean ground surface (Figure

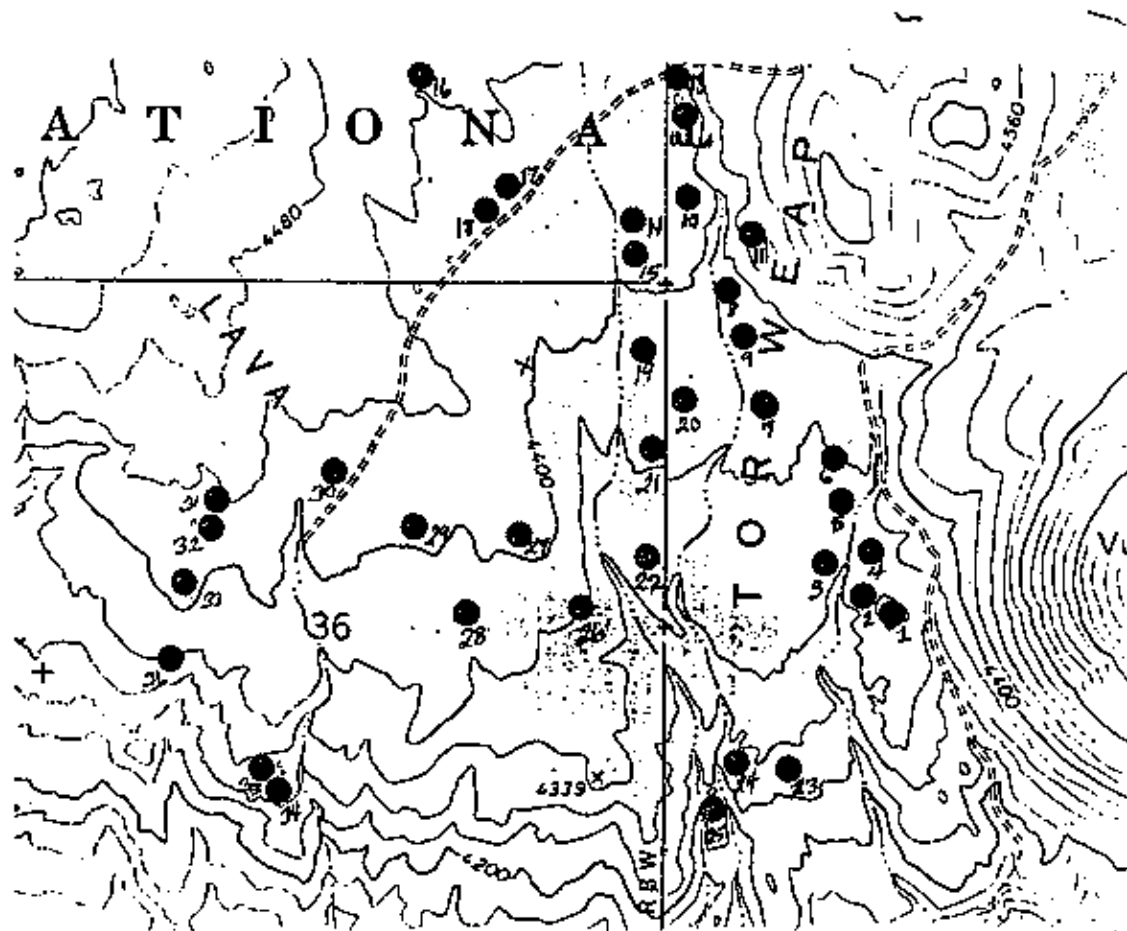


Figure 4. Map showing the location of features in the study area that were analyzed by this author.

surfaces which implies slow cooling. From aerial photographs, the features can be seen to follow a roughly arcuate northwest - southeast trend that bifurcates from the general north - south trend of the Toroweap Fault.

The features found in the Toroweap Valley have previously been viewed as pressure blisters (Hamblin and Best, 1970) that have formed in the basanitic lavas that originated from the Mount Emma area and flowed southward on the Uinkaret Plateau down to and over the north rim of the Grand Canyon. A volcanic pressure ridge is defined as, "An elongate uplift of the congealing crust of a lava flow, probably due to the pressure of the underlying and still flowing lava", according to the definition in the American Geological Institute Glossary of Geology (Gary et al., 1972). These features vary widely in dimensions. Some are ridge-like, as much as 15 meters (50 feet) in length and 8 meters (25 feet) in width, with vertical topography of up to 5 meters (16 feet) (Figure 5). Others are beehive shaped with radii varying from 4 meters (13 feet) and a vertical relief varying from 2 meters (6 feet) to >8 meters (25 feet), respectively (Figure 6). Polygonal joints and cracks, characteristic of slower cooling rather than simple subaerial cooling, are seen on some of these features (Figure 7). These indications of slow cooling of molten lava of both the ridge and conical



Figure 5. Ridge-shaped feature seen in the
Toroweap Valley



Figure 6. Beehive-shaped feature seen in
the Toroweap Valley



Figure 7. One of the numerous features that exhibit polygonal cracking

varieties are not consistent with simple subaerial pressure blisters or fissures. Given the aridity of the region likely since post-Wisconsin time and the inferred 1-2 my age, it seems unlikely that erosion could have removed more than unconsolidated ash. Thus, the polygonal jointing must be considered to be the result of slow cooling under a light ash bed that is now missing. By contrast, other features appear to be direct subaerial spatter cones exhibiting a very frothy nature without polygonal jointing. They are rich in volatiles and have been considerably weathered (Figure 8). Again, these spatter cones suggest a more hornito-like origin rather than a simple pressure blistering or ridging origin.

Some of the larger features are ridge-like with a considerable overgrowth of vegetation; surface weathering has broken off blocks of glassy skinned material. Had this been a pressure blister, one would expect to find a smooth skin on the surface of the feature and an extremely vesicular, volatile-rich lava layer beneath. These larger features did not appear to be hollow within and thus are not believed to be pressure blisters or ridges from the most recent flows but rather to be direct mantle fissure orifices.



Figure 8. Typical spatter cone feature found
the Toroweap Valley

XENOLITHIC INCLUSIONS

Most prominent in the basanite features is the presence of green and red colored peridotite inclusions enclosed within the basanite features. Their dimensions and mineralogy suggest a xenolithic origin for the basanite features, or, are inconsistent with a pressure blister origin.

The xenoliths found within the basanite features vary widely in size from < 3 cm to over 20 cm in body diagonal, the average size being around 7 to 9 cms (Figure 9). Shapewise, some are very angular while others are ellipsoidal. A statistically meaningful distribution with respect to shape or size, angularity or roundness between the different peridotites was difficult to determine because of the limited amount of sampling. Overall though, the xenoliths were found to be more rounded in nature, suggesting that they originated at considerable depth and rose with a high velocity.

The xenoliths are predominantly olivine-rich (Fo_{90-92}) with smaller amounts of ortho- and clinopyroxene present. In most samples, millimeter-sized spinel grains are also visible with the naked eye. Thus their origin may be considered to be lower crustal or upper mantle depth. The xenoliths themselves have been



Figure 9. Varied peridotite xenoliths found in basanite features in the Toroweap Valley

classified into three different textural types and a detailed discussion follows in the next section.

Compositionally, the green colored xenoliths plot as lherzolites and harzburgites (Best, 1974). The red xenoliths, on the other hand, were ignored by previous investigators, who interpreted them as being highly weathered varieties of the green xenolith (Hamblin, 1987; pers. comm). The green variety of xenolith is similar in composition to many xenoliths found worldwide: San Carlos, Az. (Weiss, 1984); Kilbourne Hole, Tx. (Carter, 1977); Tahiti (Tracy and Robinson, 1977); and South East New England (Leavy and Hermes, 1977). The descriptions given by the aforementioned researchers occasionally mention host rock-xenolith interaction, remelt textures, and/or diffusion of ions within grains, much of which is seen in this study too, but in the above literature cited, as well as many other xenolith published studies, there is no mention of any pervasive green to red visible color change in the samples, except in weathered outcrops.

Settling velocity calculation

A geophysical model was developed to evaluate the possibility of a lava flow 5-6 meters thick carrying kilogram size xenoliths 10 kilometers from their source to their current location. Stokes Law was used to compute

the static settling velocity of different sized olivine-rich xenoliths in a static lava flow of a fixed viscosity. The static settling velocity was then applied to Newton's Laws of motion to evaluate the distance covered and the time required before the different sized xenoliths would settle to the base of the lava flow. A computer program was written by this author in GW-BASIC (see Appendix I) to determine the distance covered and the time taken for settling of xenoliths in a basanite flow.

Assumptions

To make the model sufficiently realistic without introducing too many variables, some assumptions were made, given the gentle slope of the Toroweap Valley:

1) The aa-type lava flow behaves in a laminar manner and turbulence does not occur within the flow.

2) The velocity of the flow is constant from the time of eruption which is at least a fair approximation given the gentle slope of the Uinkaret plateau.

3) The lava is assumed mobile.

4) The temperature is assumed steady from eruption until the time it spills over the rim. Geologically sensible temperatures for such lavas vary between 1120°C and 1200°C. The viscosity over this temperature range also varies. As temperature decreases, viscosity

increases and the result would be a retardation of motion. Values of viscosity for different temperatures are obtained from literature. Viscosities considered vary between 300 and 800 poises.

5) Despite the fact that the flow may be slowing due to the gentle gradient and temperature losses of cooling, it is nevertheless assumed that the xenoliths are constantly accelerating when within the flow. This is possible if one considers that the force of gravity attracts the xenolith at a constant acceleration. The data used for the evaluation of the settling velocity were obtained from various sources (Clark, 1980, Ryan and Blevins, 1987).

Method of calculation

To obtain the settling velocity of any sample, the equation used was:

$$V = (2 \times R \times dD \times g) / (9 \times N)$$

where,

V = settling velocity of the basanite flow unit in
cm/s

R = effective radius of the xenolith within the
basanite flow unit in cms

dD = the density difference between the basanite and the xenolith to be considered in g/cm^3

g = acceleration due to gravity = 980 cm/s^2

N = viscosity of the basanite unit in poises.

R was determined assuming that every sample was a perfect ellipsoid and the major axis was measured for each xenolith. It was found to vary between 2 cms and 10 cms.

dD was obtained from literature (Clark, 1980). The density of basanite was assumed to be 2.774 g/cc and the density of peridotite to be 3.234 g/cc , yielding a difference of 0.46 g/cc .

N was determined for different temperatures using values from literature (Ryan and Blevins, 1987). A non-linear relationship exists between the viscosity and temperature for different lavas (Figure 10). Therefore three viscosities at different temperatures were considered to evaluate the settling velocities of the peridotite xenoliths (300, 500 and 800 poises corresponding to 1120°C , 1150°C and 1200°C respectively).

To evaluate the distance and time at which a given xenolith would settle to the base of a lava flow, the laws of motions were applied. The total thickness of the flows is believed to be about 265 meters (1400 feet) with each individual flow being no thicker than 6 m (20 feet)

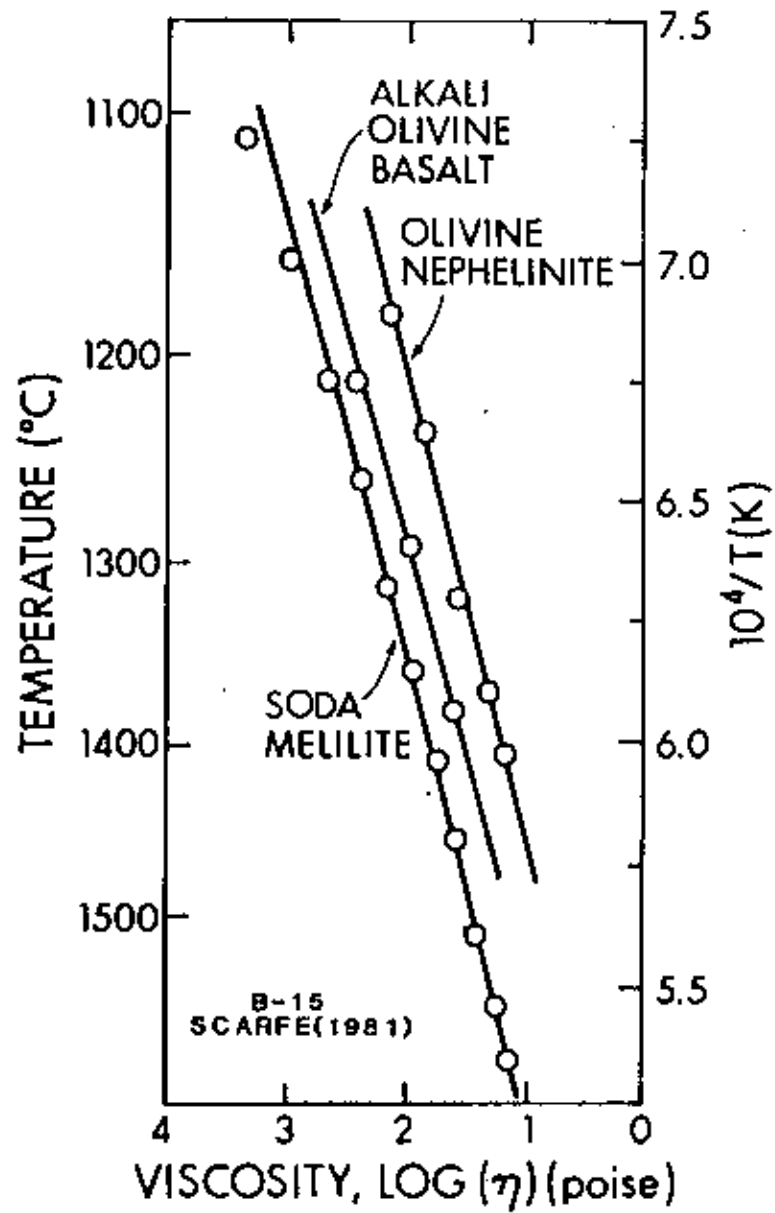


Figure 10. Plot of Viscosity vs Temperature for an alkali olivine basalt lava (Scarfe, 1981; in Ryan and Bevins, 1987)

(Hamblin, 1974).

For a given xenolith, the net downward acceleration can be calculated as,

$$a = (V_s/t) \quad I$$

where,

a = the net acceleration due to gravity on the xenolith, 980 m/s^2

V_s = the settling velocity of the xenolith (cm/s)

t = time taken for the xenolith to reach the base of the individual flow, in seconds.

Also, from the laws of motion,

$$h = \frac{1}{2} a t^2 \quad II$$

where

h = the thickness of the flow in meters

Therefore, substituting in I,

$$h = \frac{1}{2} (V_s/t) t^2$$

$$t = 2h/V_s$$

Since t is herein defined as the xenolith settling time, then the distance d_x that the xenolith travels before having settled out can be evaluated as

$$d_x = V_x t$$

where,

V_x = the velocity of the lava flow in the horizontal direction.

Discussion of results

Results of this analysis indicate that the xenoliths could not have travelled in lava flows from Mount Emma, 10 kilometers away (Table 1). Even xenoliths with a 2.5 cm radius would not be carried more than half a kilometer from the source. The assumptions introduced in the calculation simplifies the model considerably, but the result is unlikely to change by as much as an order of magnitude. A xenolith in a lava flow < 6 meters (20 feet) thick would sink to the base of the flow much before it reached the Canyon end of the Toroweap Valley (Figure 11). If the xenoliths were carried in the flow, and they were settling in the viscous medium, they would presumably be found at the base of the flow. Field evidence shows

TEMPERATURE (°C)	VISCOSITY (poises)	DISTANCE TRAVELLED (meters)
1120	800	797
1150	500	498
1200	300	298

Radius of xenolith: 1 centimeter
Thickness of flow: 6 meters
Velocity of flow: 300 meters/hour

Table 1:
The maximum distance travelled by a xenolith
settling in a flow moving at a fixed velocity

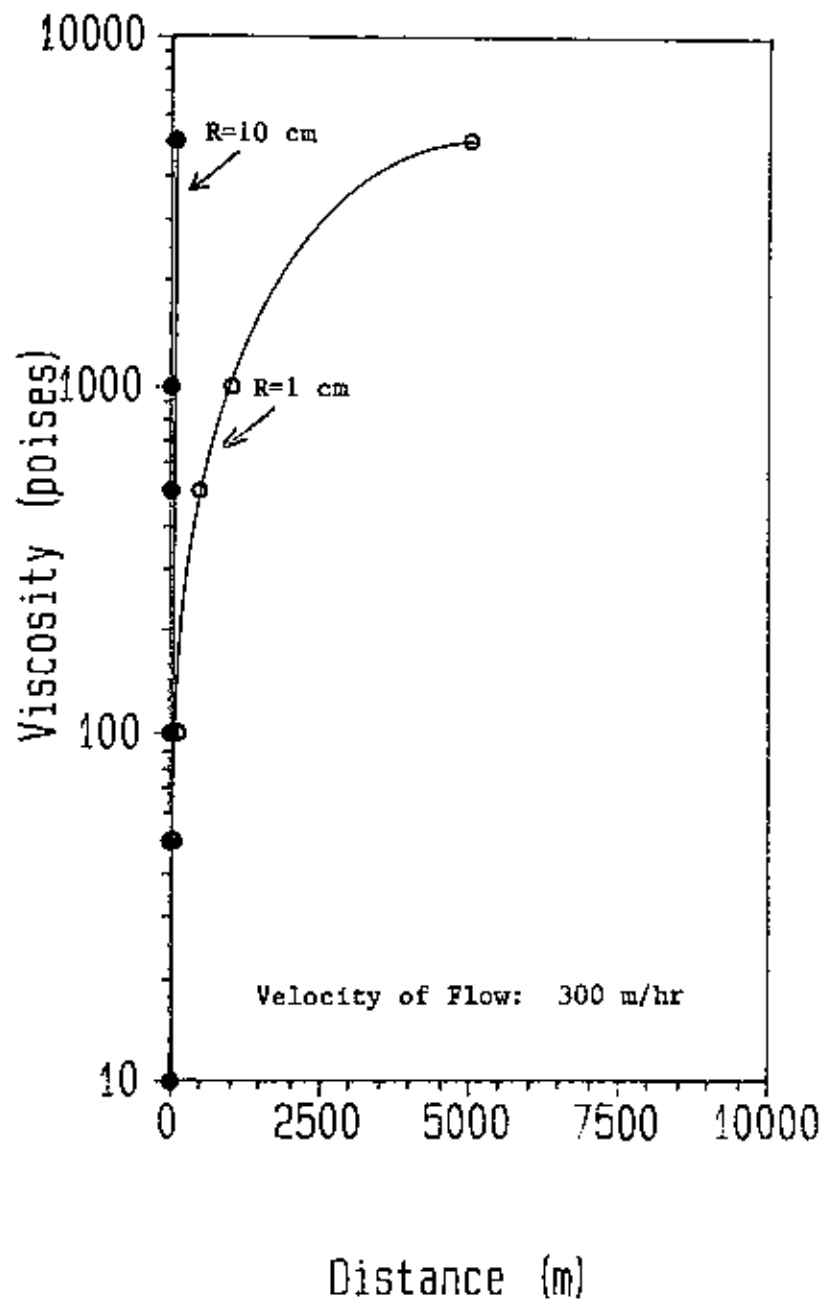


Figure 11. Viscosity vs Distance travelled for xenoliths in a basanite lava

that these xenoliths are scattered randomly throughout the features. Therefore it would be impossible to transport xenoliths of the size and density considered to the canyon end of the Toroweap Valley from vents around or at Mount Emma, 10 kilometers away. The numbers in Table 1 show that regardless of the viscosity, velocity, and xenolith radius values, the xenoliths found in the field could not have entirely originated from the distant vents of Mt. Emma or Mt. Trumbull, at least 14 kilometers (10 miles) away. The largest xenolith (10 kg, maj axis: 23 cm) was found within 150 m of the canyon rim in an igneous feature that exhibited polygonal cracks ! While this xenolith was exceptionally large, a large percentage (> 90%) of the more normal sized xenoliths are shown, by this computation, not to be related to either Mt. Emma or Mt. Trumbull.

Another hypothesis thus needs to be proposed to possibly explain the origin of the volcanic features. Two alternative scenarios can be envisioned:

A. The source of the lava flows is much nearer the canyon rim in the Toroweap Valley. This would account for the features being pressure blisters, but may not account for the xenoliths being scattered randomly within the features. As defined earlier a volcanic pressure ridge is

"An elongate uplift of the congealing crust of a lava flow, probably due to the pressure of the underlying and still flowing lava". Pressure ridges are also commonly oriented perpendicular to the flow direction of a given lava flow. If the pressure blisters are analogous to pressure ridges, their orientation may be oriented. The lack of systematic orientation of the volcanic features seen in the Toroweap Valley (Figure 2) thus reduces the likelihood of them being flow-related pressure features. In addition, this scenario does not account for the various morphologies of the features seen in the Toroweap Valley.

B. The features are direct mantle orifices that have punctured the crust in the Toroweap Valley and erupted under ash, cinder or thin bedded lava cover that has meanwhile been eroded to expose those features. The ash, cinder or thin bedded lava cover can be assumed given the highly volcanic nature of the entire area during the Late Cenozoic. These original covers would have possibly resulted in the retardation of the lava extruding from the orifice and hence localize the basanite around the features. This inferred cover would allow intermediate cooling rates for the polygonal joints developed in many of the features. If these covers were thinner or absent,

the lava would have probably spread over a larger area and all the features would be hornitos, and remnants of large lava fountains would have been likely. Hence, if it is assumed that the cover on the Toroweap Valley is not uniformly thick, the various morphologies may be explained.

CHEMISTRY OF THE BASANITE FEATURES

Introduction

The X-ray fluorescence technique was used to obtain major oxide content of nine preselected basanite samples from volcanic features within the Toroweap Valley and four alkali olivine basalts from Vulcan's Throne. The aim was to study variations that may exist within the samples from the Toroweap Valley itself, between the Valley and Vulcan's Throne, and to compare the results obtained with published results of Best and Brimhall (1974). The basanite is believed to originate from volcanic vents in the Mount Emma region. The alkali olivine basalt is found characteristically on Vulcan's Throne (Best and Hamblin, 1970). The age relationship makes the alkali olivine basalt older than the basanite, and it has also been

suggested that, since the compositions of the two lavas are so close, they are consanguineous, having formed as a result of limited partial melting in the upper mantle (Best and Brimhall, 1974). Samples for this analysis were obtained from different features spread across the East-West width of the Toroweap Valley (see Table 2 and Figure 2) and from four locations on Vulcan's Throne.

X-ray fluorescence method

X-ray fluorescence was performed on the thirteen preselected samples using a Diano 8300 device at Franklin and Marshall College, Lancaster, PA, under the guidance of Mr. Steve Sylvester.

The samples selected for this analysis were xenolith-free assemblages of texturally glassy basanite and alkali olivine basalt from the Toroweap Valley and Vulcan's Throne, respectively. Each representative sample was powdered to finer than 80 mesh in a porcelain lined shatter box. A weight of $3.6000\text{g} \pm 0.0002\text{g}$ of lithium tetraborate was then weighed and intimately mixed with $0.4000\text{g} \pm 0.0001\text{g}$ to maintain a 9:1 ratio. With a couple of drops of lithium iodide added as a flux, the mixture was then fused over a Meeker burner at about 1000°C . The fused mixture was then poured into a platinum dish and quenched. Once cooled, the sample was marked and loaded

for analysis.

Figure 12 is a schematic representation of a typical X-ray fluorescence spectrometer. In the DIANO 8300, a 50 kilovolt accelerating voltage with a 40 milliamp sample current is applied to a tungsten-chromium target that emits primary X-rays. This X-ray source is collimated to impact the fused sample, which in turn emits its own secondary x-ray fluorescence, characteristic of the elements that it is composed of. The secondary fluorescence is passed through a collimator and strikes the analyzing crystal at a known angle theta. The analyzing crystal used in this analysis is a Lithium Fluoride (200) crystal with a d-spacing of 4.02 Å. The advantage of using this crystal is that the best intensity of the reflected wavelength is obtained for the elements that are analyzed. The analyzing crystal diffracts according to the Bragg equation:

$$nL = 2d \sin \theta$$

where n is the order of diffraction (normally 1), L is the wavelength in angstroms, d is the interplanar spacing of the analyzing crystal in angstroms, and theta is the angle between the incident radiation and the crystal surface.

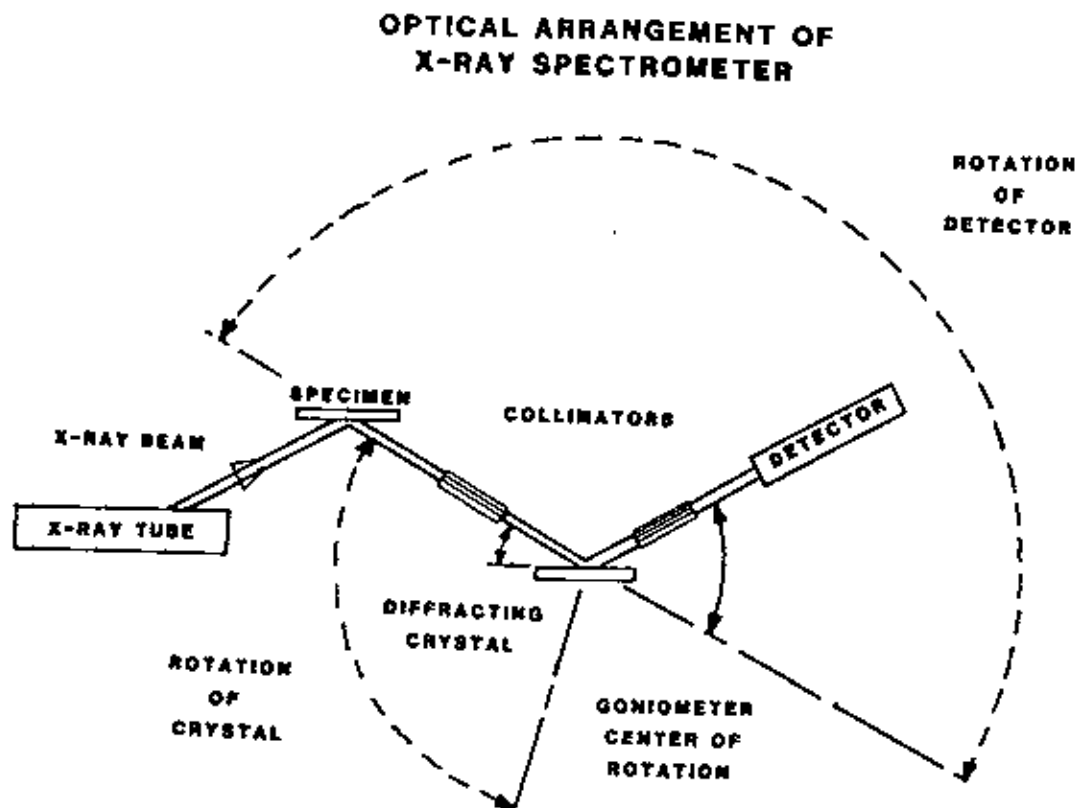


Figure 12. Schematic representation of an X-ray fluorescence spectrophotometer

The intensity of the diffracted radiation is measured by a scintillation detector and is converted to a percentage composition of each element as a function of intensity. The device is computer-interlocked and analysis is initiated using a software package "EXSOFT" marketed by DIANO.

The results obtained are listed in Table 2.

Since the analysis calculates Fe as total iron, wet chemical analysis for ferrous iron was undertaken. Each sample was digested in a mixture of concentrated HF + concentrated H_2SO_4 in a porcelain crucible and then titrated versus potassium permanganate ($KMnO_4$). The volume of potassium permanganate solution of known normality is used to calculate the equivalent atomic weight of FeO (the ferrous content) in the sample.

Next the Loss on ignition (LOI) was determined for each sample.

About 1.0000 g of sample was heated in a platinum crucible at a temperature of 900°C for 50 minutes in air. The dehydrated sample was then re-weighed and the percentage loss of water was determined as a correction for oxidation of ferrous iron.

Discussion of Results

The total standard deviation observed for the major

TOROWEAP VALLEY SAMPLES:

<u>SAMPLE</u>	<u>SiO2</u>	<u>TiO2</u>	<u>Al2O3</u>	<u>FeO</u>	<u>Fe2O3</u>	<u>MnO</u>	<u>MgO</u>	<u>CaO</u>	<u>Na2O</u>	<u>K2O</u>	<u>P2O5</u>
H1B	42.76	2.66	13.39	5.81	6.89	0.18	10.66	10.22	2.98	1.38	0.69
H61	43.54	2.66	13.61	9.70	2.47	0.17	9.94	10.27	3.66	1.61	0.72
H6-1	41.35	2.59	12.77	7.70	5.66	0.20	10.16	10.16	2.73	1.58	1.45
H11-4	43.48	2.57	14.00	7.75	4.22	0.17	10.68	10.06	3.89	1.32	0.73
H11-6	43.73	2.74	13.62	8.69	3.95	0.18	9.87	10.04	3.81	1.66	0.74
H14A-2	44.18	2.62	13.71	8.13	3.95	0.17	9.94	10.41	3.23	1.52	0.70
H17-A	42.75	2.50	13.04	8.23	2.95	0.17	10.66	10.93	3.03	1.58	0.66
H18*	44.36	2.69	13.73	8.27	4.22	0.17	9.97	10.15	3.87	1.36	0.78
H30	43.37	2.61	13.49	9.30	2.76	0.18	10.02	10.40	3.99	1.65	0.71
H36	43.66	2.70	13.64	5.82	6.91	0.17	10.08	10.30	3.67	1.64	0.79

VULCAN'S THRONE SAMPLES:

<u>SAMPLE</u>	<u>SiO2</u>	<u>TiO2</u>	<u>Al2O3</u>	<u>FeO</u>	<u>Fe2O3</u>	<u>MnO</u>	<u>MgO</u>	<u>CaO</u>	<u>Na2O</u>	<u>K2O</u>	<u>P2O5</u>
F1-1	45.66	1.81	13.74	6.58	3.48	0.16	12.15	10.75	3.06	1.22	0.64
VT52	45.34	1.54	12.00	5.11	5.27	0.15	15.94	9.99	2.29	0.90	0.56
VTWF4	45.23	1.69	12.70	6.46	3.90	0.16	14.40	10.29	2.56	1.21	0.63
LP6	42.56	2.16	13.05	4.82	7.21	0.17	12.78	10.91	2.63	1.21	0.75

BASALTES FROM THE WESTERN GRAND CANYON:

<u>SAMPLE</u>	<u>SiO2</u>	<u>TiO2</u>	<u>Al2O3</u>	<u>FeO</u>	<u>Fe2O3</u>	<u>MnO</u>	<u>MgO</u>	<u>CaO</u>	<u>Na2O</u>	<u>K2O</u>	<u>P2O5</u>
AV34	44.9	2.4	13.60	12.3*	----	----	10.5	9.9	3.4	1.6	----
UK1	45.35	2.25	13.59	12.36*	----	----	10.84	9.83	3.28	1.44	----

* Fe calculated as total FeO.

For location of the Toroweap Valley samples see Figure **.

Vulcan's Throne samples obtained from random locations on the cinder cone.

AV34: Average of 34 basanites from the western Grand Canyon (Best and Brimhall, 1974).

UK1: Average basalt composition from the Uinkaret Plateau (Hamblin and Best, 1970).

Table 2

Results of X-ray fluorescence analysis

oxides of the reference samples is no greater than 0.65 weight percent, and thus the results are considered reliable. Table 2 lists the average compositions of the samples analyzed. Two analyses for each sample were made and the average was calculated.

Figure 13 shows a significant cluster of points between 2.5 and 2.8 wt % TiO_2 . An envelope can be drawn around nine points, all of which are values from the basanite features located all across the Toroweap Valley. The remaining four values represent TiO_2 weight percentages of the Vulcan's Throne samples obtained randomly across Vulcan's Throne (Hanson, Perscomm). The features are distinguished by their higher TiO_2 content and lower MgO/FeO ratio when compared with the Vulcan's Throne samples. A third set of values are those obtained for average basanites from the Western Grand Canyon region. These have been obtained from literature sources (Hamblin and Best, 1970; Best and Brimhall, 1974). The values here lie outside the range of the Toroweap Valley features and are intermediate between the latter and Vulcan's Throne samples. The cluster of the Toroweap Valley basanites suggests a more oxidized source region for the basanite. This may imply that the basanite is a product of fractionation of alkali olivine basalt. The two lavas are known not to be coeval, but the linearity of

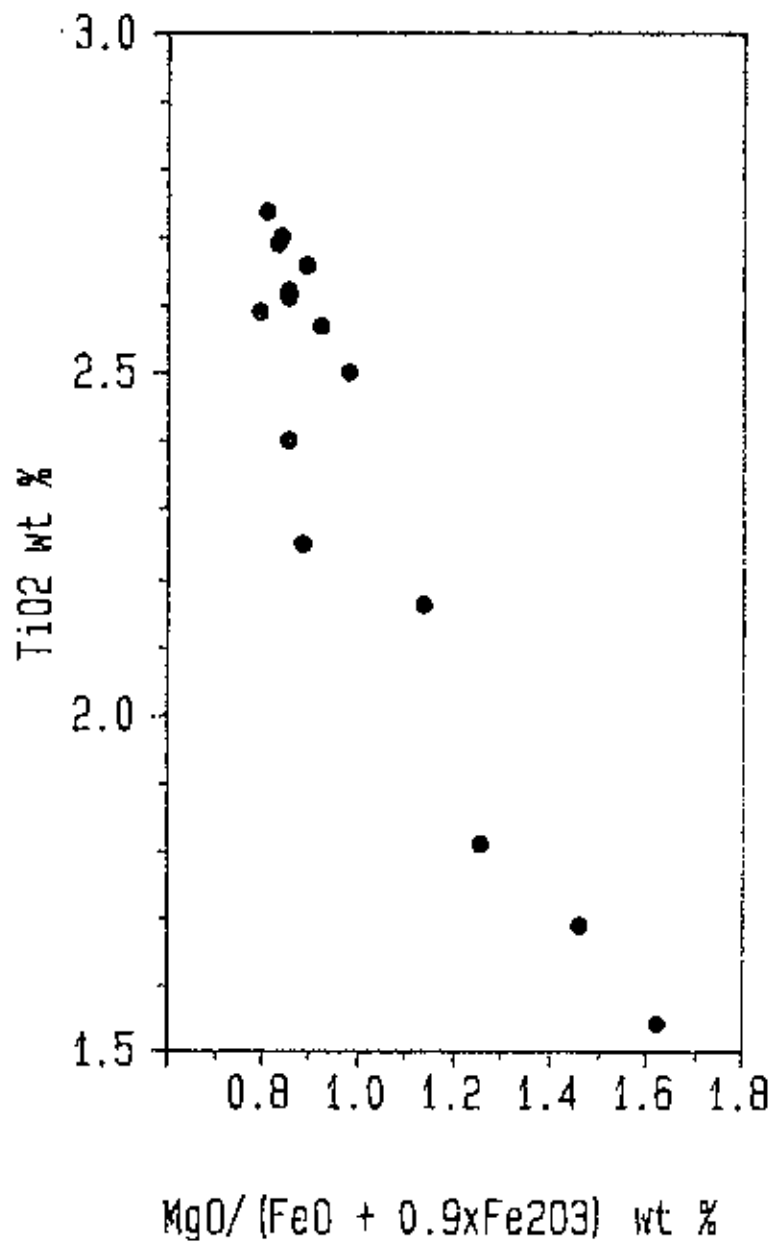


Figure 13. Variation diagram of TiO₂ vs MgO/(FeO + 0.9Fe₂O₃) for samples from three locations in the Western Grand Canyon region (see text for details)

the data suggest a possible consanguinity of source. This is possible as the alkali olivine basalt is believed to be older than the basanite (Best and Brimhall, 1974).

Figure 14 shows a similar distribution, with a cluster around the Toroweap Valley features and a wide scatter of the Vulcan's Throne samples. In contrast to the TiO_2 variation diagram, the MgO wt % values of the basanites obtained from literature lie within the Toroweap Valley feature results. This appears to support the idea that one lava (basanite) evolved from the other (alkali olivine basalt).

Between the Toroweap Valley features and the Toroweap Valley flows (Figure 15), the latter show a depletion in CaO. Though this difference is only 0.2 weight percent, the the lower values suggest a more primitive origin for the Toroweap flows. If the flows and the features had the same origin, this variation would not exist. This seems to indicate a consanguinity between the alkali olivine basalt from Vulcan's Throne and the basanite from the Toroweap Valley features, but as is described later, all the regions may be consanguineous.

The chemical data suggest that the Toroweap Valley features are all derived from the same magma chamber or source area. The Vulcan's Throne and Toroweap Valley lavas are not known to be coeval, but the characteristic

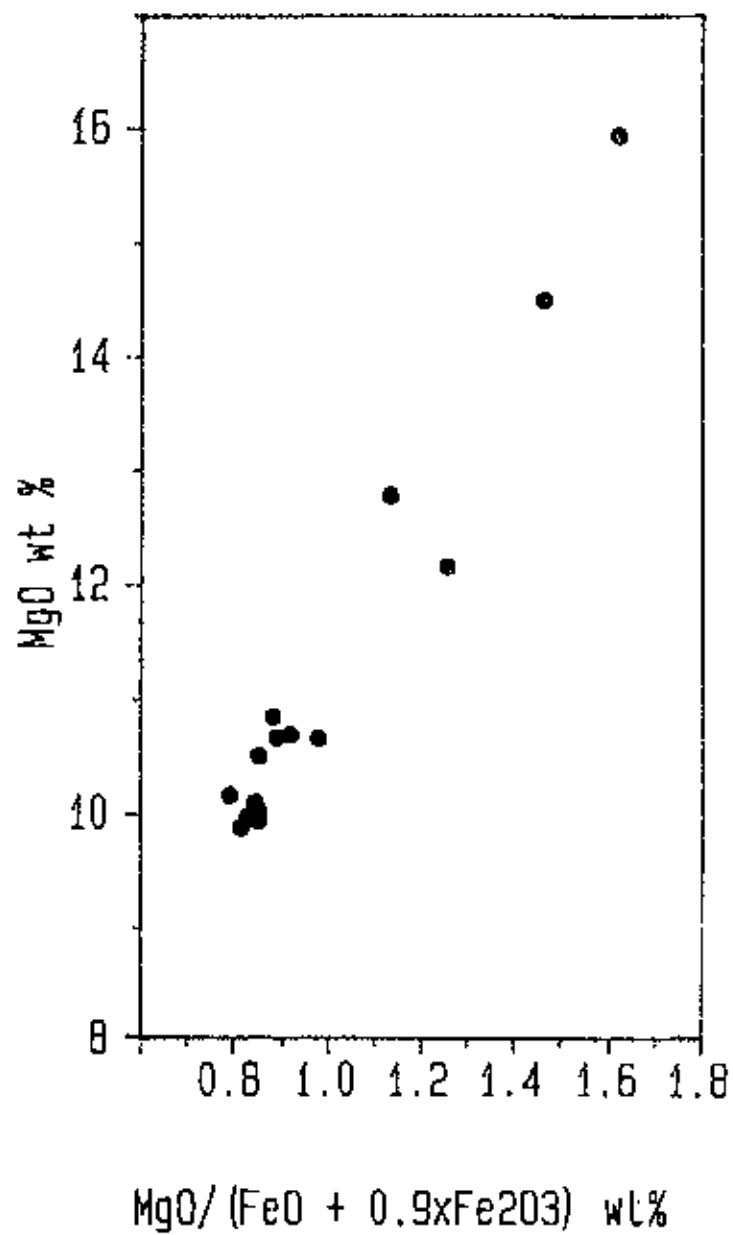


Figure 14. Variation diagram of MgO vs MgO/(FeO + 0.9Fe₂O₃) for samples from three locations in the Western Grand Canyon region (see text for details)

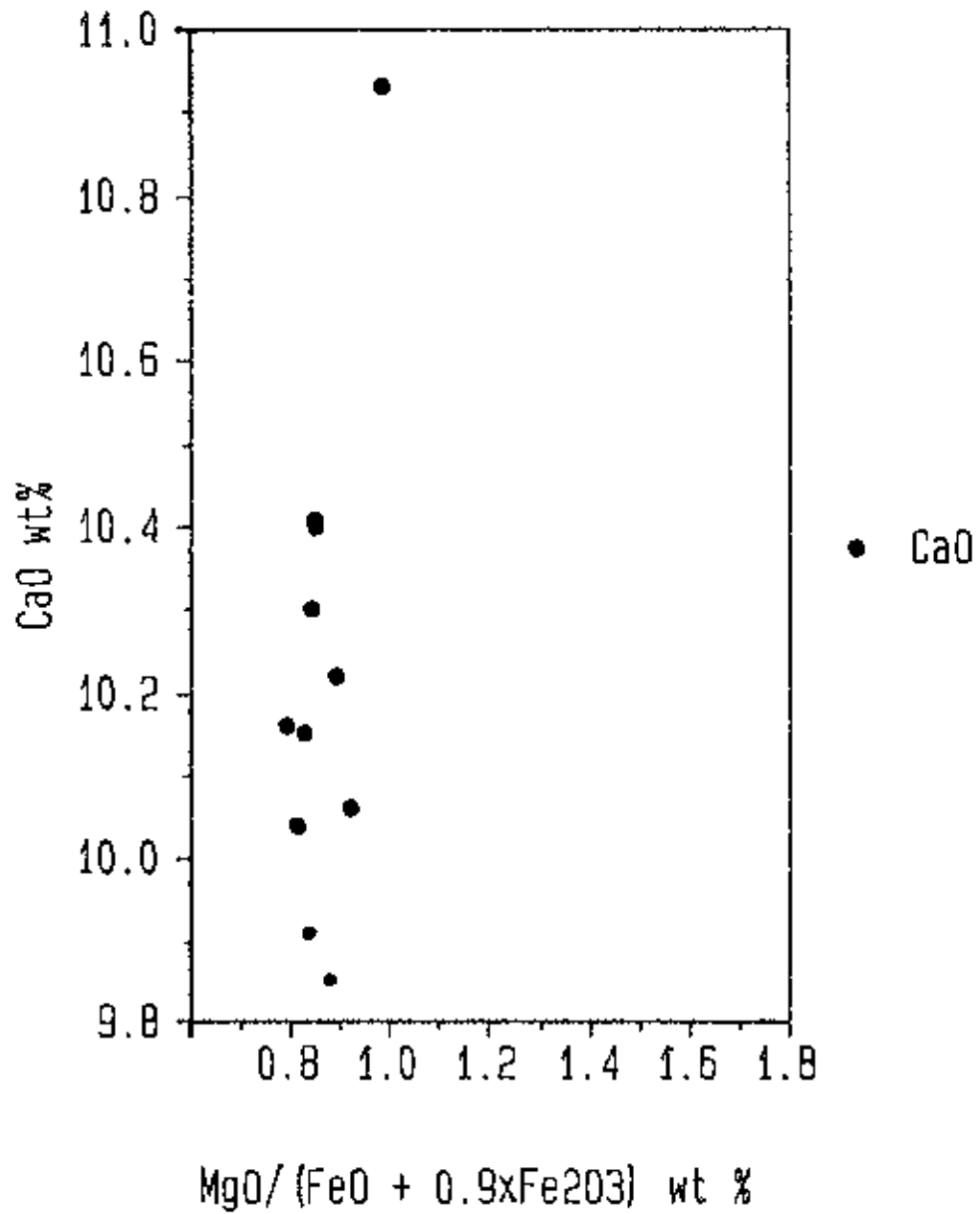


Figure 15. Variation diagram of CaO vs MgO/(MgO/FeO + 0.9Fe₂O₃) for samples from three locations in the Western Grand Canyon region (see text for details)

linearity of the data suggests a possible consanguinity of source for the above two areas as well as the Toroweap features. The possibility of Vulcan's Throne and the features in the Toroweap Valley being related is supported by the fact that both areas show both green and red colored xenoliths, which, from field work done by this author in three locations upto 10 kilometers away from the Toroweap Valley, are not found. By, comparison, the basanite flows in the Toroweap Valley show minute (about 0.5 cm in diameter) xenoliths enclosed in the flows. A comparison of the chemistry of the Toroweap features and the Toroweap lava flows fails to suggest any major genetic differences between the two. A map of the Uinkaret basalts (Figure 16) shows the source of the Toroweap flows to be at least 10 kilometers north of the Toroweap features. Thus a separate orifice for the Toroweap Valley flows is invoked, considering the different volumes of lava generated. A sufficiently large magma chamber may provide an adequate amount of lava to both regions as shown in Figure 17. This would necessarily place the magma chamber at considerable depth (>50 km?). From the mineralogy of the enclosed xenoliths, this is probably true. No conclusive distinction could be made for the basanite samples from within the Toroweap Valley. This may be attributed to the small sample population size that

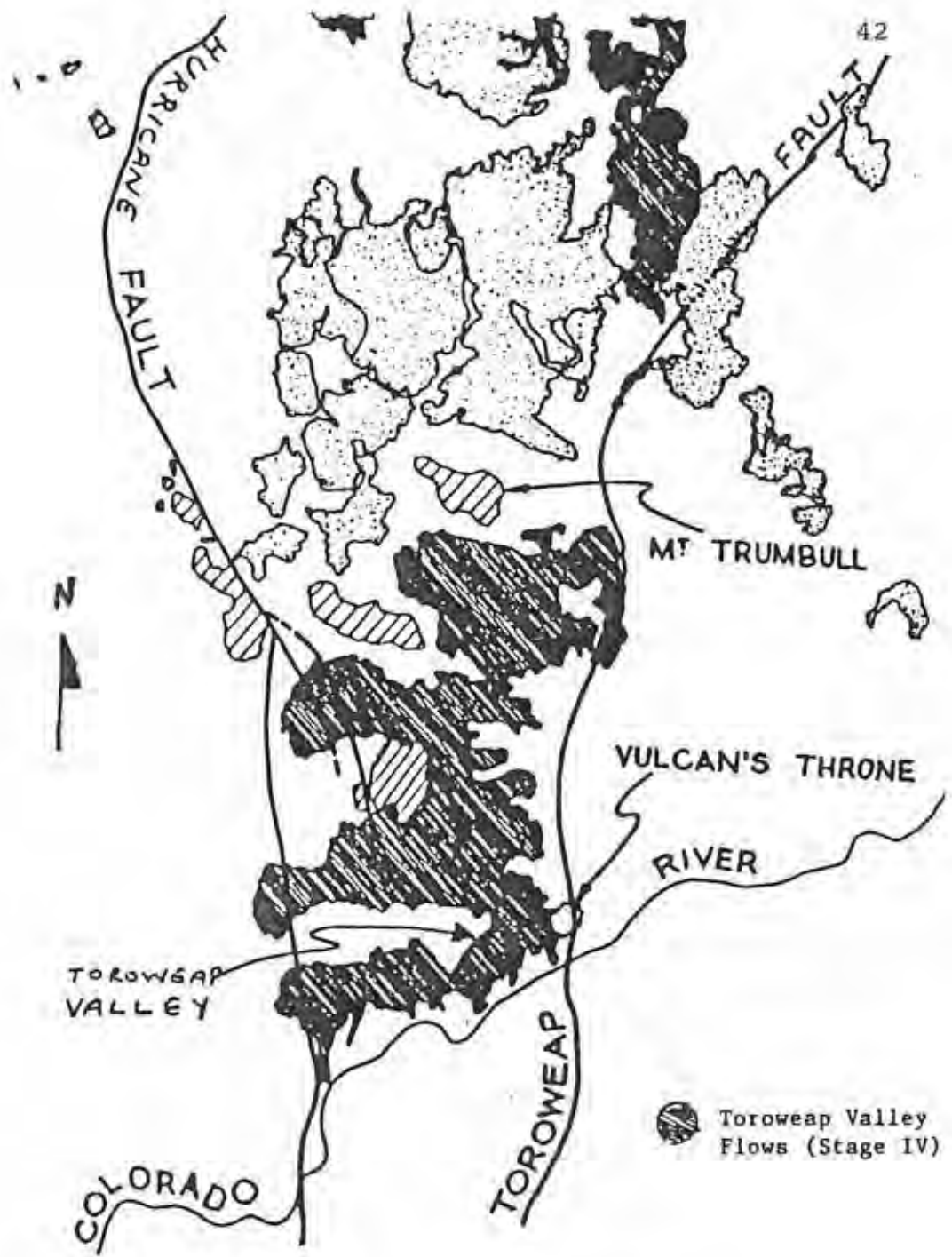


Figure 16. Map of the Toroweap Valley area representing the extent of localized basanite flows (adapted from Hamblin, 1974)

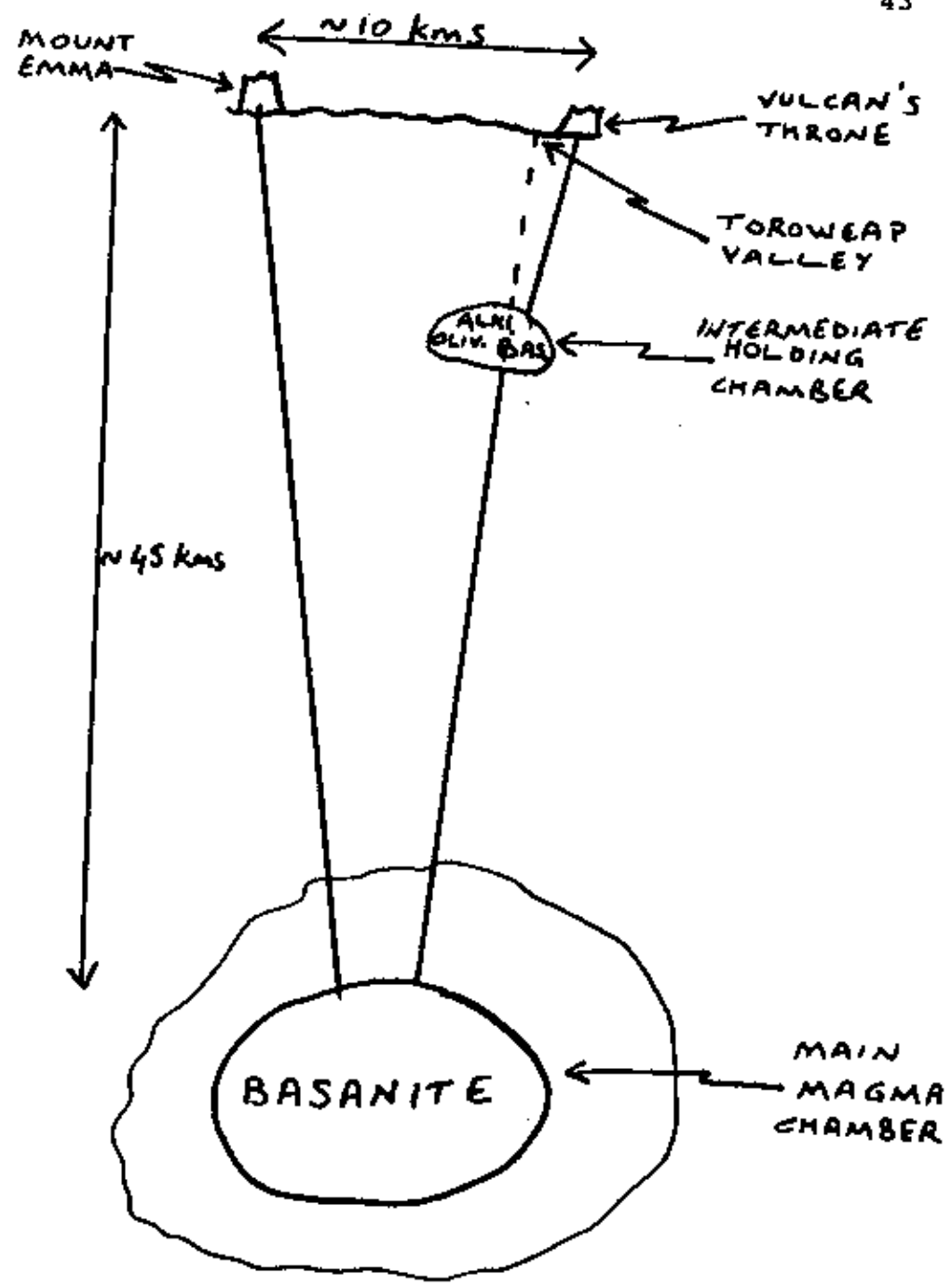


Figure 17. Cartoon representing the proposed relationship between the Toroweap Valley, Vulcan's Throne and Mount Emma

was analyzed. On the other hand, since the sample locations were scattered across the Toroweap Valley, any major chemical difference would be manifest in a wide scatter of oxide percentages. In fact, a tight envelope can be drawn around these samples that may even suggest that all the features formed at the same time, namely during one eruptive even.

HYPOTHESIS OF ORIGIN

A linearity exists between the basanite oxide percentages of the Toroweap Valley features and the alkali olivine basalt from the Vulcan's Throne lavas, suggesting a consanguineous relationship between the two. There is no distinguishable major element variation seen in the oxide percentages from the Toroweap features and the Toroweap Valley flows, suggesting a common source for the features and the Valley flows. Between the alkali olivine basalt and the basanite, the latter is of a more primitive nature (Figure 18). Age dating of the basanite and the alkali olivine basalt (Best and Brimhall, 1974) indicates that the basanite is younger in age. Thus, to explain this apparent discrepancy between chemical trend and isotopic age dating, the following model is proposed and

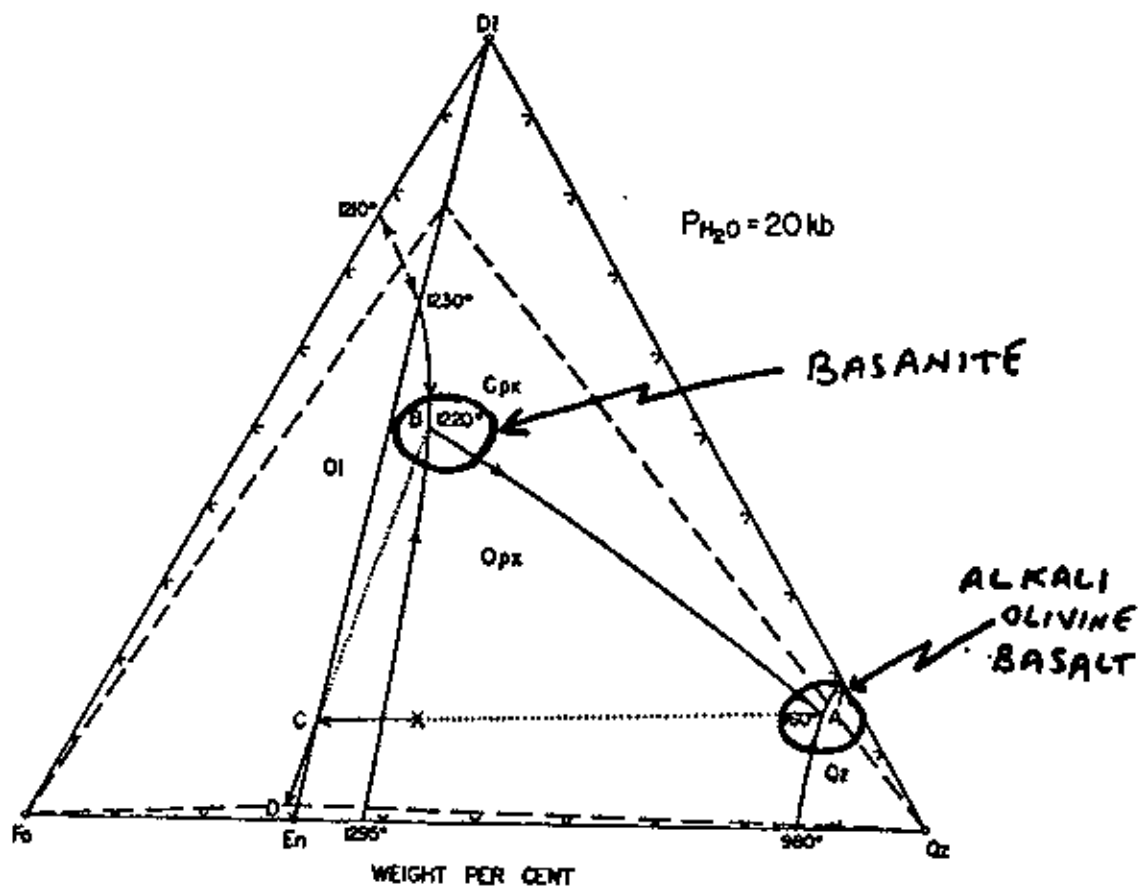


Figure 18. Ternary phase diagram showing the crystallization sequence of alkali olivine basalt and basanite (from Yoder, 1969)

illustrated in Figure 17.

A sufficiently large parental magma chamber of basanitic composition is located at a depth of at least 45 kilometers (depth obtained from geothermobarometric calculations; Geothermobarometry, this study). From this chamber, a significant amount of magma was transported to an intermediate holding chamber at shallower depth. The lower temperature in this holding chamber initiated differentiation of the basanitic magma, thus yielding a magma enriched in alkali content. Periodic eruptions from this holding chamber resulted in the formation of the alkali olivine basalt cinder cone Vulcan's Throne. Peridotite xenoliths, brought to the holding chamber from the parental magma chamber had the time, oxidizing conditions and a sufficiently high temperature to induce oxidation and a resulting color change of many xenoliths from green to red in color.

Subsequently, the parental magma chamber erupted, transected the differentiated holding chamber below Vulcan's Throne, and punctured the surface in the Toroweap Valley as the basanite features that are now visible. These basanite features enclose both green and red colored peridotite xenoliths which are not seen elsewhere in the region. The parental magma chamber was also the source of the lavas that originated in the vents around Mt. Emma

that are of basanitic composition.

SUMMARY OF RESULTS

Over one hundred and fifty "Pimple-like" igneous features are found scattered in an arcuate manner trending roughly Northwest-Southeast in the Toroweap Valley.

The basanite features show a variety of sizes, presence of polygonal joints and cracks, and presence of upto kilogram-size peridotite xenoliths enclosed within the features. A settling velocity calculation proves that a 2 centimeter xenolith carried by a basanite lava flow cannot be carried over a distance of 10 kilometers in a 5-6 meter thick lava flow without settling to the base of the flow first.

Literature available on the Toroweap Valley and its environs (Hamblin and Best; 1970, for example) does not mention the occurrence of peridotite xenoliths in the surrounding areas. Since peridotite xenoliths of various sizes are found only in basanite features from the Toroweap Valley, it can be presumed that the features carried the xenoliths up from lower crustal or upper

mantle depths when they erupted.

The peridotite xenoliths enclosed within the basanite features are green and red in color, varying in size from 2 centimeters to over 15 centimeters in diameter. The two types of xenoliths are compositionally identical and suggest that the Toroweap Valley features are either of lower crustal or upper mantle origin.

Trends seen in the oxide contents of samples analyzed from the Toroweap features, the Toroweap Valley flows and the flows from Vulcan's Throne suggest a consanguineous relationship between the three regions. Isotopic age dating (Best and Brimhall, 1974) indicates that the alkali olivine basalt is younger in age than the basanite lava flows and the basanite features. A phase diagrammatic relationship (Yoder, 1969) shows that the basanite is a parental magma whereas the alkali olivine basalt is a magma derived from the basanite.

A genetic model is proposed wherein the basanite from the Toroweap features and the Toroweap flows originate from the same magma chamber whereas the alkali olivine basalt from Vulcan's Throne originates from an intermediate holding chamber whose magma originated from

the parental magma chamber.

ANALYSIS OF PERIDOTITE XENOLITHS

PETROGRAPHY

Introduction

The xenoliths found on the Toroweap Esplanade have characteristics which are similar only to a limited extent when compared with those found on Vulcan's Throne. An earlier section (Settling Velocity) shows that it is not possible for a basanite lava flow 6 meters thick to carry xenoliths for over 10 kilometers without the xenolith settling out of the mobile lava first.

It has also been discussed that Vulcan's Throne and the Toroweap Valley are not known to be coeval, but that they may be consanguineous.

Thus to test the possibility that xenoliths found in the Toroweap Valley are related to the Vulcan Throne xenoliths, a detailed petrographic analysis was undertaken and the results compared with those obtained from a similar study of Western Grand Canyon xenoliths by Best (1974).

Best (1974) classified the xenoliths on a textural basis and defined three distinct types of olivine rich xenoliths.

Type G was used to describe granoblastic silicate xenoliths that have crystals generally 1-3 mm in diameter and which lack foliation. They are composed of dark-green diopside, dark-brown to black enstatite, pale yellow-green olivine and jet-black spinels. Well developed kink-bands are described in the olivines, and the pyroxenes showed slight strain manifest by uneven extinction.

Type P closed xenoliths are harzburgite-lherzolite nodules that are characterized by prismatic, green to gray-brown poikiloblastic enstatite as large as 25mm X 6 mm. These grains are usually surrounded by smaller pale-yellow olivine and inconspicuous diopside (~ 2 mm). The olivines found in these xenoliths are generally unstrained with well developed 120° triple-boundary grain margins. Typical are two-pyroxene intergrowths parallel to (100).

Type M (megacrystals) harzburgite nodules have been characterized by large turbid enstatite megacrystals that are pearl-gray in hand sample and stand out as prominent equant grains in a finer grained, non-foliated matrix (<2mm) of glassy, pale yellow-green olivines and inconspicuous diopsides. The turbid appearance is caused by brown, sub-micron sized platelets aligned in (010). Spinel, phlogopite and possible amphibole were suspected but not confirmed.

Initially a macroscopic analysis was undertaken on similar samples from the Toroweap Valley based on visible textural differences in an attempt to apply Best's classification scheme. The texture and features described by Best were not identified by this author. Thus a primary classification scheme was developed based on a macroscopic evaluation, followed by a microscopic evaluation to verify and add to the existing database. The samples used for this study were peridotite nodules found within individual features in the Toroweap Valley.

Thin sections from the area were made and studied using transmitted light, and polished sections were analyzed in reflected light. Reflected light proved to be an effective way of studying the textures of opaque minerals and the alteration characteristics of all the phases.

Host rock-xenolith interaction was difficult to study within the scope of this thesis using transmitted light because of the glassy nature of the basanite. Though it is not covered in this study, this author believes that this interaction is important in understanding the nature of the upper mantle and further detailed analysis will add substantially to the volume of knowledge in the field.

There were three aims kept in mind when petrographic analysis was undertaken:

1. To look for homogeneity or heterogeneity between the xenoliths of the field area,
2. To study similarities or differences that may occur within the study area and the adjacent Vulcan's Throne, and
3. To interpret color changes that occur within the green xenoliths.

Sample Preparation

Unoriented rock chips were sliced using a Buehler silicon carbide saw, ground with 1000 mesh grit and cemented (using an epoxy resin) to the frosted side of a glass slide. The glass slide was frosted to improve the contact between the rock chip and the glass surface. The chip was trimmed and polished down to thirty microns (0.03 mm) using silicon carbide grit of successively finer grain size followed by alumina powder for a final polish. A polarization color chart served as a guide to determine the thickness of each slide using index minerals. For a more detailed description, the reader is referred to Hutchinson (1974).

Rock chips were cut in an identical manner as described above with the size of each chip having dimensions averaging 1.5 cm x 1.5 cm x 1 cm. The chips were then mounted in a bakelite ring and cemented to the

inner rim of the disks using a casting resin. The ring was then polished with successively finer diamond pastes and finally with 0.5 micron Al_2O_3 powder to obtain the highest reflectivity.

Classification and mineralogy of xenoliths in the basanite features

As described earlier, an attempt to classify the Toroweap Valley xenoliths using Best's textural classification scheme proved unsuccessful and thus this author developed a classification scheme that envisions four textural types of xenoliths based on macroscopic and microscopic analyses. It should also be noted that this classification scheme is unique to the Toroweap Valley peridotite xenoliths, and thus needs to be tested against xenoliths from other localities in the Western Grand Canyon region.

TYPE G* (granoblastic) (Figure 19) xenoliths typically show a granoblastic texture, similar to the type G xenoliths described by Best, but differ mainly in that the grain size in the TYPE G* from the Toroweap Valley is smaller by one order of magnitude. In hand sample, this type is characterized by turbid euhedral megacrysts of orthopyroxene measured upto 10 mm in length, the average size is about 5mm. The matrix of this type appears

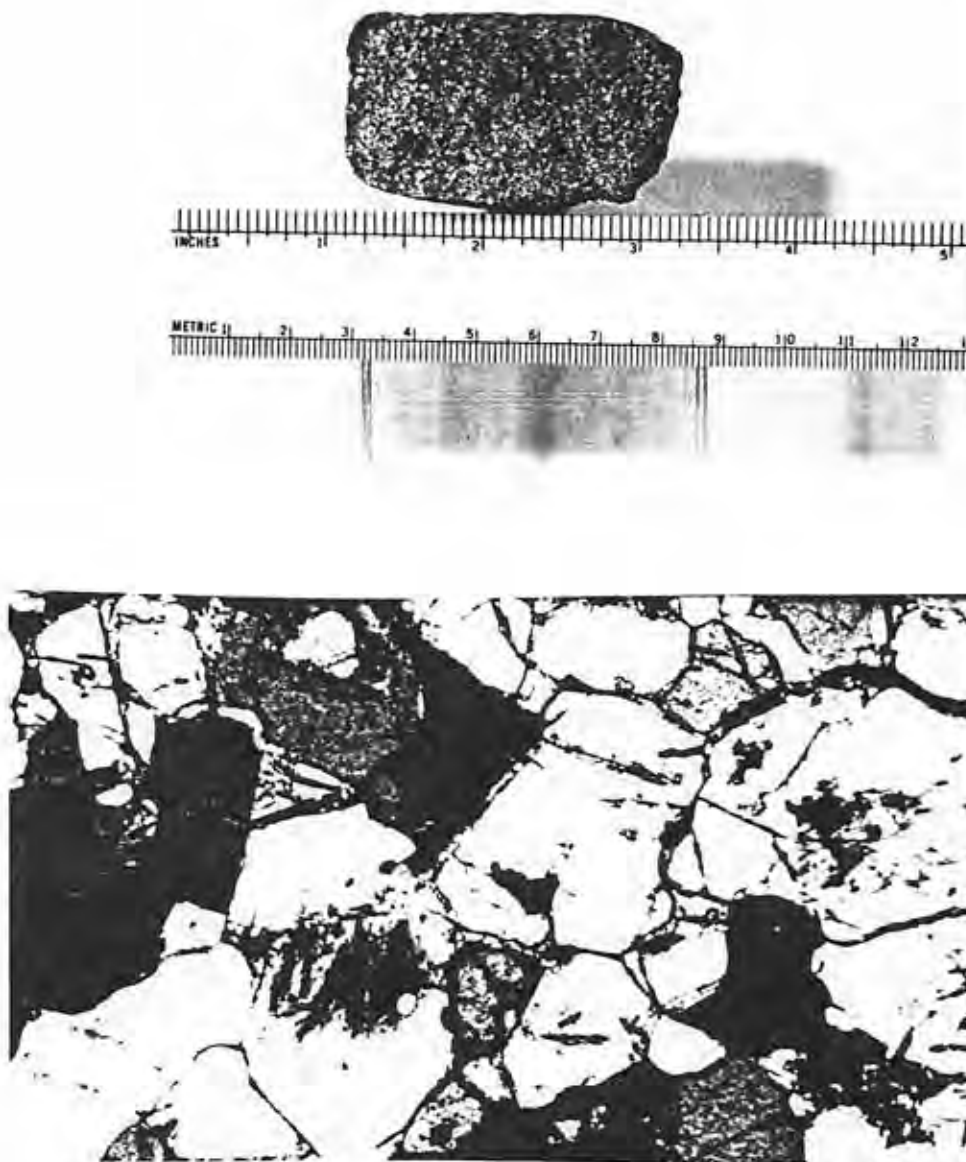


Figure 19. TYPE G* xenolith in hand sample (above) and
in thin section (below) (XPL, 5.5 mm across)

non-foliated in hand sample and thin section and is comprised of equigranular silicates (olivine and clinopyroxene) 1-2 mm in diameter. Jet black spinels appear as black specks disseminated throughout all the samples of this type. In addition, many of the spinels appear brownish in color suggesting an alteration of the original phase. A majority (>50 %) of the red colored xenoliths collected exhibit this texture (see later section on Red Xenolith analysis).

Microscopically, the xenoliths are found to be olivine-rich with variable amounts of large orthopyroxene grains (μ 6mm) and trace amounts of clinopyroxene (<5%). The average grain size of the olivine is 1-2 mm. Spinels, brown in color and translucent in nature are scattered throughout the rock. They occur both poikilitically enclosed within the silicate phases as well as along grain boundaries. From microprobe analysis these spinels are found to be chrome- and aluminum rich and lacking in iron, which may cause their translucency. Turbid enstatites compare with those found in Best's Type M xenoliths. Macroscopically, a true distinction could not be made between Best's Type G and Type M for the samples from the Toroweap Valley.

TYPE C (Cataclastic): This group of xenoliths shows a typical cataclastic texture (Pike and Schwarzman, 1977)

that is visible to the naked eye. This type is characterized by discontinuous strands of spinel that pervade the peridotite. A linear fabric is easily seen across the specimen. The individual silicate grains are seen to orient themselves parallel to the strands of spinels (Figure 20). The spinels here are found both within silicate phases and along grain boundaries. The largest silicate seen is clinopyroxene, 1-1.6 mm in diameter. The texture seen here is similar to the Type G* described earlier, but the Type 'C' xenolith shows a definite fabric that pervades the entire specimen. The grain size of this type is typically smaller.

TYPE F (Friable): This is the rarest type of xenolith that was found in the Toroweap Valley. They comprise about 5 percent of the samples seen in the Toroweap Valley. These xenoliths are highly granular in texture and friable, similar to the Group I xenolith found at San Carlos (D. W. Weiss, pers. comm.). The grain size of this type is similar to that of Type C. It is possible that this type is simply a more intensely deformed Type C xenolith or the friable nature may even be a result of severe weathering effects.

Type P xenoliths, described by Best were not found in the Toroweap Valley, and those found on Vulcan's Throne

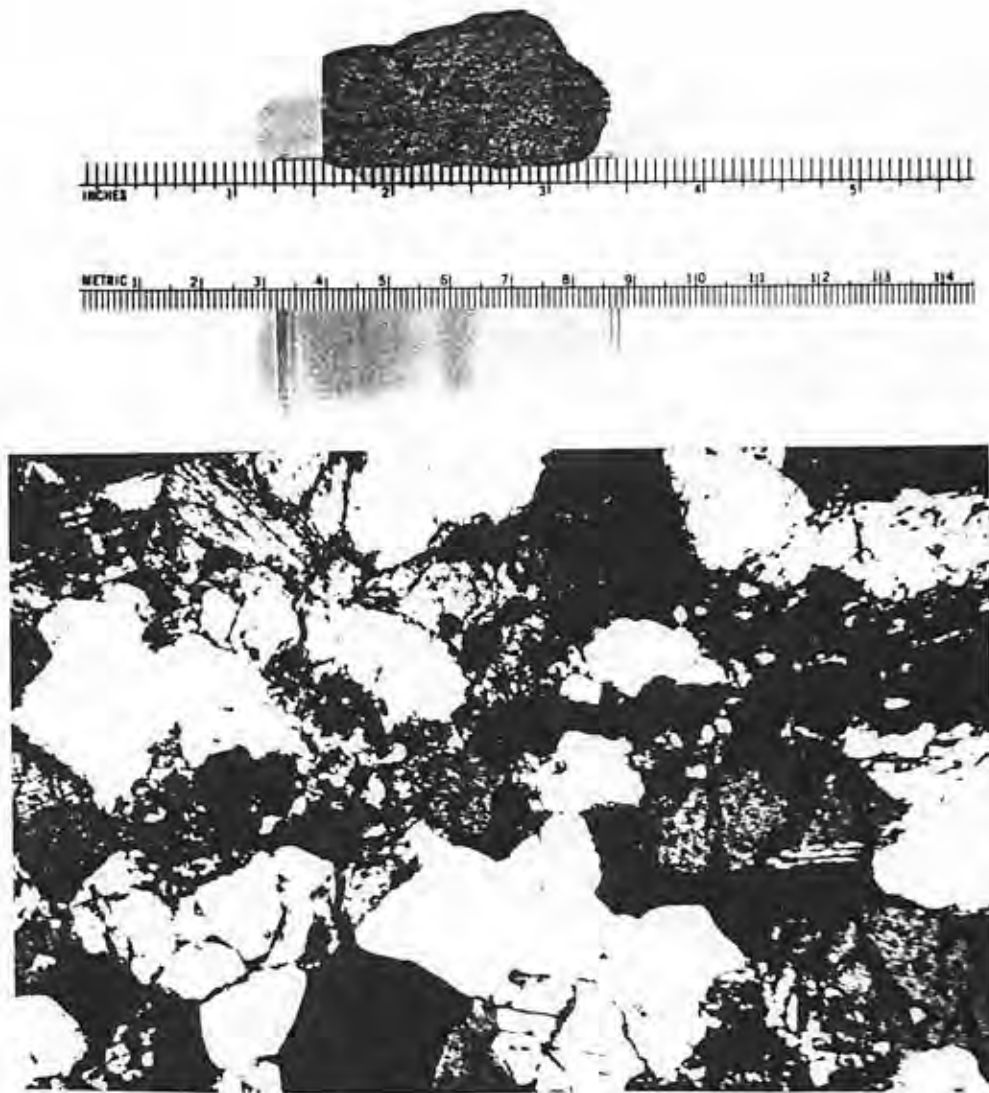


Figure 20. TYPE C xenolith in hand sample (above) and
in thin section (below) (XPL, 5.5 mm across)

are red in color (Hanson, pers. comm.).

Reheating of xenoliths

A very important aspect of the field relation is that red and green colored xenoliths occur side by side in the same eruptive vent feature. Thus, weathering as a sole cause of reddening can probably be ruled out. It is possible, conceivably, that a given flow carrying "virgin" green xenoliths, picked up weathered red xenoliths from an earlier episode to end up with a flow containing both red and green xenoliths. However, observations at 1500 meters (5000 feet) on Vulcan's Throne of green and red colored xenoliths in a flow horizon within just meters of the summit of the cinder cone would argue that the red and green xenoliths probably even erupted simultaneously. What is considered a likely explanation is that the volcanic pipe carrying "virgin" green xenoliths transected a second magma chamber at shallower depth that contained red xenoliths that changed color in a more oxidized environment than subaerial cooling and/or weathering could have provided (see Hypothesis of origin; previous section). To test this hypothesis, chips of green-colored peridotite xenoliths were heat treated under controlled conditions at various in the laboratory, and the resulting samples were then visually studied. Further detailed

analysis involving reflectance infrared analysis has been deferred to a specific study to be presented as a sequel to this treatise.

Method developed to reheat xenoliths

This reheating process was developed by the author in an attempt to study the compositional changes of the visibly green colored xenoliths under conditions that may have existed during the time of eruption of the lavas on the Toroweap esplanade and thus relate these changes with the possible origin of red colored xenoliths seen in the field.

Samples were heated at various temperatures and environments in a Pt₈₀Rh₂₀ resistance furnace. The desired temperature was maintained using a Leeds and Northrup Electromax temperature controller with an accuracy of $\pm 3^{\circ}\text{C}$ (See Figure 21).

Temperatures for a basanite lava-country rock interface rarely exceed 600 to 650°C (T.M. Lutz, personal communication, 1988). Thus 650°C was considered the maximum temperature that a basanite lava could reach at the contact between the lava and the ground surface.

Two environments were simulated, one to study the changes at 1 atmosphere pressure in a free-flowing air atmosphere, and another at 1 atmosphere in carbon

SCHEMATIC OF FURNACE USED FOR REHEATING EXPERIMENTS

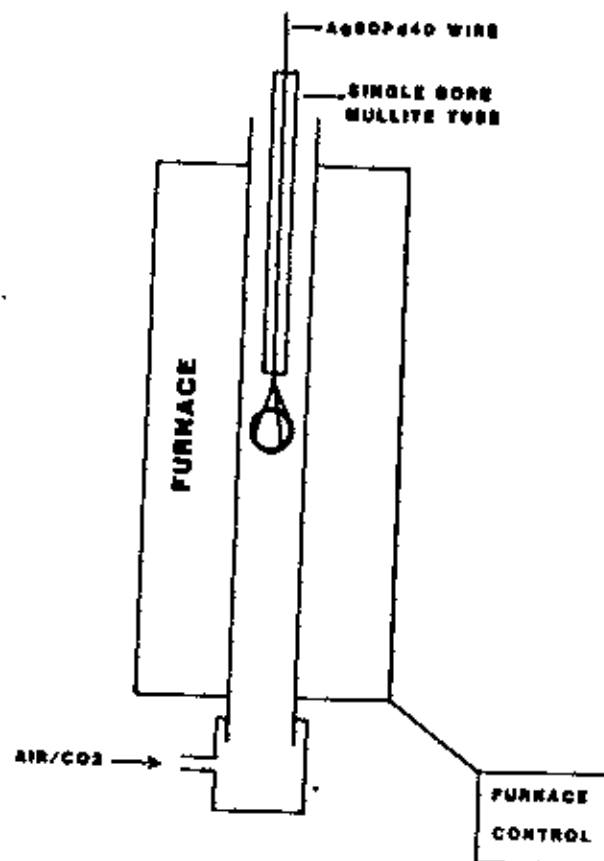


Figure 21. Schematic representation of furnace used to reheat green colored peridotite xenoliths

dioxide. The air atmosphere was used to mimic subaerial conditions and carbon dioxide was the ambient gas used for conditions chosen to simulate (FMQ) buffer conditions, assuming that the xenoliths were enclosed in a basaltic magma of (FMQ) redox potential (an assumption supported for example by Haggerty et al., 1969). The CO₂ gas was monitored using a two stage regulator and the rate of flow maintained at 4 cc/sec which was determined as an optimum flow rate to completely saturate the sample and prevent backflow of air from the surrounding atmosphere into the furnace (Nafziger et al, 1971).

Chips of green xenolith approximately 1.5cm X 1.5cm X 0.5cm were cut from non-friable green xenoliths of all types with a Buehler diamond micro-saw. The chips were air dried at 25°C for at least 8 hours and then suspended at a preset temperature in the furnace at one atmosphere pressure. The sample sat in a glazed porcelain ring suspended by Ag₆₀Pd₄₀ wire passed through a double bored mullite rod to increase rigidity and reduce chances of tipping during the experiment.

The sample was held in the furnace for predetermined time periods. The samples were then air quenched and studied in reflected light and visually with the naked eye.

Discussion of results

Figure 22 shows the changes that were seen for one xenolith heated under different conditions. A burnt appearance can be seen on the more extremely heated samples, but no true red color is visible. When the samples heated in CO_2 were examined, it was found that though heated for a prolonged time at a high temperature (1250 hours at 450°C), a change as great as that seen in the air treated sample was not visible. This would be expected, considering the lower oxidizing conditions created in a CO_2 -rich atmosphere. Figure 23 shows the changes that are seen for this specimen before and after heat treatment.

It is thus believed that if the time-temperature space constraints are extrapolated, there would be some condition under which the green phase would become visibly red. It is worth emphasizing however, that the 1250 hour/ 450°C heating in air does not redden the sample. Hence weathering can essentially be ruled out as the reddening process. Preliminary reflected infrared analysis (more sensitive than the eye) indicates that alteration occurs with even the slightest reheating.

Red-colored xenoliths in thin section

Introduction

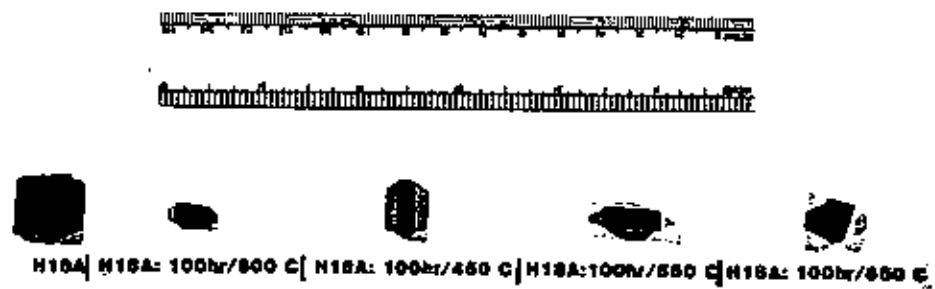


Figure 22. Green colored xenolith heated in air for different time periods and temperatures

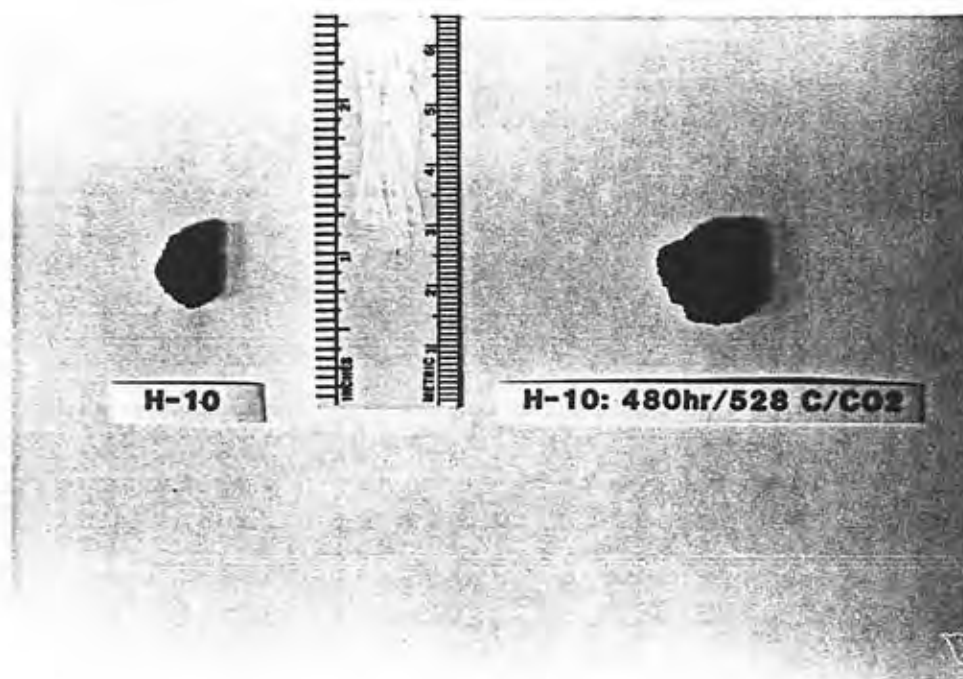


Figure 23. Green colored xenolith before and after heating in CO_2 gas

Figure 24 illustrates the two types of xenoliths found in the Toroweap Valley (and on Vulcan's Throne). The visibly red colored xenoliths found in the Toroweap Valley are generally of the textural Type G*. (Figure 25). Specimens of the other types commonly show a slight discoloration in certain specimens, but none was visibly "eclogite-red" like Type G*. The red coloring is seen predominantly in the olivine grains and is not visible in the orthopyroxene. Clinopyroxene shows discoloring in red colored samples, but true red coloring of the clinopyroxene phase remained unconfirmed.

The cause of the coloring could be as a result of simple weathering of olivine, but this idea was suspect after green and red colored xenoliths were found within 10 centimeters of each other in the same flow near the summit of Vulcan's Throne (Ulmer, pers. comm., 1988) and a similar case was seen in the Toroweap Valley. Had the reddening been a result of simple weathering, both xenoliths might be expected to be red in color. The flows showed only surface weathering and from the nature of the sharp red and green colors through the xenoliths, weathering could not be considered the cause of the color change, unless picked up from a previously weathered flow. The section on heat treatment however argues strongly against this possibility. Reheating of the green

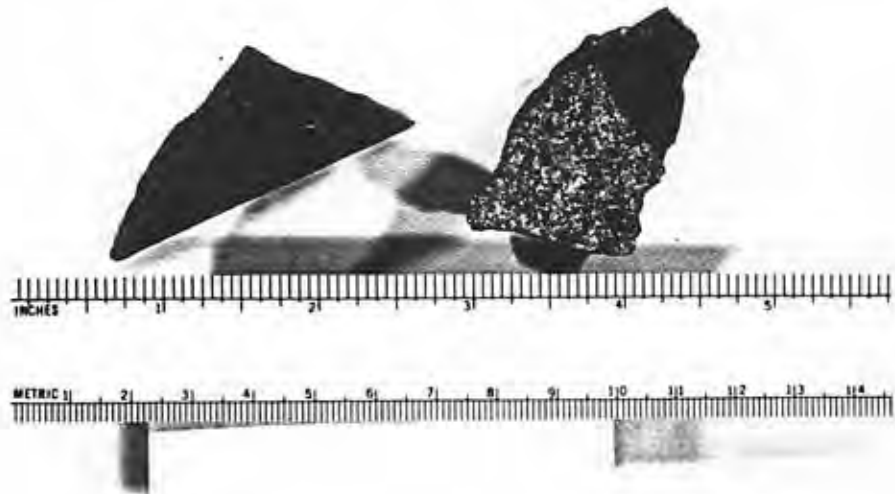


Figure 24. Hand samples of red and green colored xenoliths



Figure 25. Sample of red colored TYPE G* xenolith

xenoliths was attempted to simulate, under controlled conditions, the changes that might have occurred in the xenoliths. The changes seen in the reheated samples suggest that this alteration is a result of reheating of the original green xenolith.

When red colored xenoliths were analyzed in thin section, it was found that the color change was pervasive through the entire olivine, thus refuting the idea that the color change is a surface weathering phenomenon. Other silicate phases and spinels are also found to change in composition (see below). Thus another cause needs to be envisioned. It is believed that the changes seen are a result of compositional changes in the olivines (for example, Haggerty et al., 1967; Schaefer, 1983) caused by reheating of the original sample. This petrographic analysis describes the changes that are seen in the red xenoliths. Interpretation of the compositional changes seen will follow in a future publication. In thin section, changes are observed primarily in olivine and spinel and these changes are that are believed to be the major cause of the color change.

Alteration of Olivine

In plane-polarized light, a red phase occurs within the olivine that is preferentially oriented parallel to

the principal crystallographic directions. In thin section, this phase appears as strands that extend toward the core of the mineral grain from the margins (Figure 26). These strands are similar to the symplectic intergrowths described by Haggerty and Baker (1967). The red phase is also pleochroic in nature, showing a color change from red to pale orange. Olivines also show a blue tinge in plane-polarized light when the red strands are oriented North-South or East-West on the microscope stage. This "Schiller-like" effect may be a result of two superimposed effects on the olivine grain resulting from orientation of the red streaks. When light is vibrated parallel to the c-axis, an orange tint can be seen; when light is vibrated perpendicular to the c-axis a red or blue tint is visible. This pleochroic nature is typical of red xenoliths. The red color in olivine is concentrated around the margin of the grain. Very rarely can a completely red core be seen. Secondary red strands are seen oriented perpendicular to the primary strands (Figure 27). The fact that this phase is not randomly oriented suggests a crystallographic control on development and nucleation of the red phase.

Red coloring is also seen in the grain boundaries and fractures of all the silicate minerals in the red xenoliths. The nature of this coloring cannot be

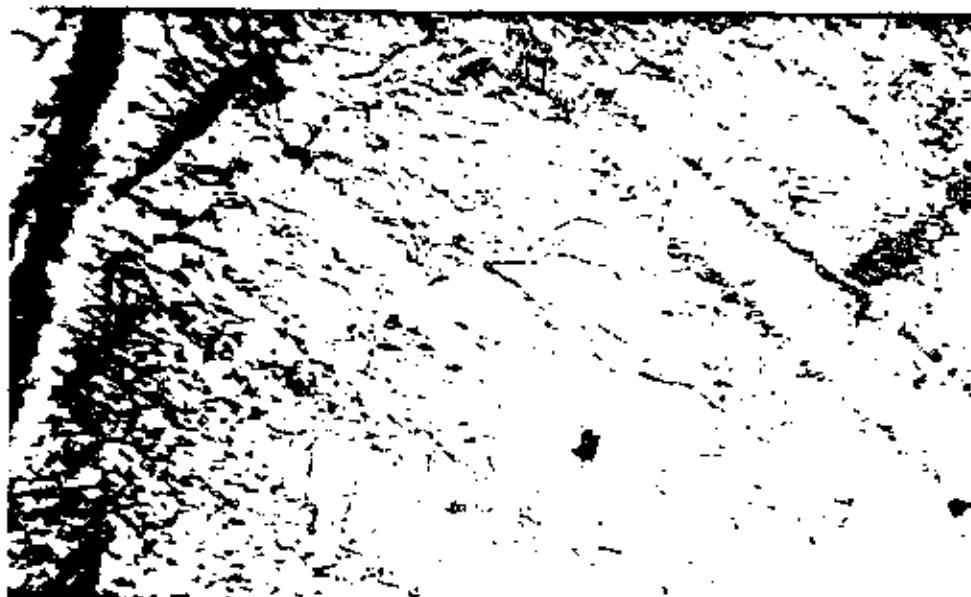


Figure 26. Photomicrograph of ferric-rich red strands
found within red colored olivine
(PPL, 1 mm across)



Figure 27. Photomicrograph of secondary ferric-rich strands oriented perpendicular to primary strands in red colored olivine (PPL, 2 mm across)

determined within the magnification used for the study because of the dense nature of the phase. The red phase is visibly deep red, almost opaque in many cases.

The nature of red coloring seen in the altered olivines is not believed to be a result of simple weathering. Microprobe analysis as well as petrographic analysis show that the green colored olivine has a Fe_{88-92} composition. Microprobe analysis of red colored olivine produces identical results. Yet there is an obvious visual difference between the two. Reheating of originally green xenoliths in controlled environments indicate that changes in the individual minerals do occur, and that these changes are not related to weathering effects. Heated at $650^{\circ}C$ for 100 hours in air, the olivine grains discolor to a turbid dark-green to brown color. This change is believed to be a result of the change in the ferrous/ferric ratio in the olivine structure. This change has been extensively studied by Schaefer (1983). She observed the changes in Fayalite-rich olivines, whereas all the changes seen in this study are seen in forsterite-rich olivines. The ferric-rich phase is known by many names depending on its true chemical composition and is commonly called Ferrifayalite (Ginsburg, 1962) and/or Laihunite (Laihunite Research Group, 1976,1982). It is believed that the red

phase seen in the olivine is, at least in part, laihunite that has formed by alteration of the ferrous ion in forsteritic olivine.

Spinel and their alteration

The spinels, viewed in both transmitted and reflected light, are found to show features typical of altered spinels (exsolution lamellae, coronas). Their nature in the peridotite xenoliths appears to have a significant bearing on the red coloring of the entire specimen.

In plane-polarized light, brown or black spinels occur along grain boundaries or poikilitically enclosed in the silicate phase. Those occurring poikilitically enclosed in silicates are mainly reddish brown in color whereas those formed along grain boundaries are both black and brown in color. The black spinels are anhedral in form and are often located in highly fractured zones within any given sample (Figure 20). Many spinels along grain boundaries appear opaque in plane polarized light, but when viewed, in condenser-enhanced transmitted light, a lighter core can be seen with a dark crust surrounding the grain (Figure 28). This crust or corona is believed to have formed as a result of reaction with the surrounding phases.

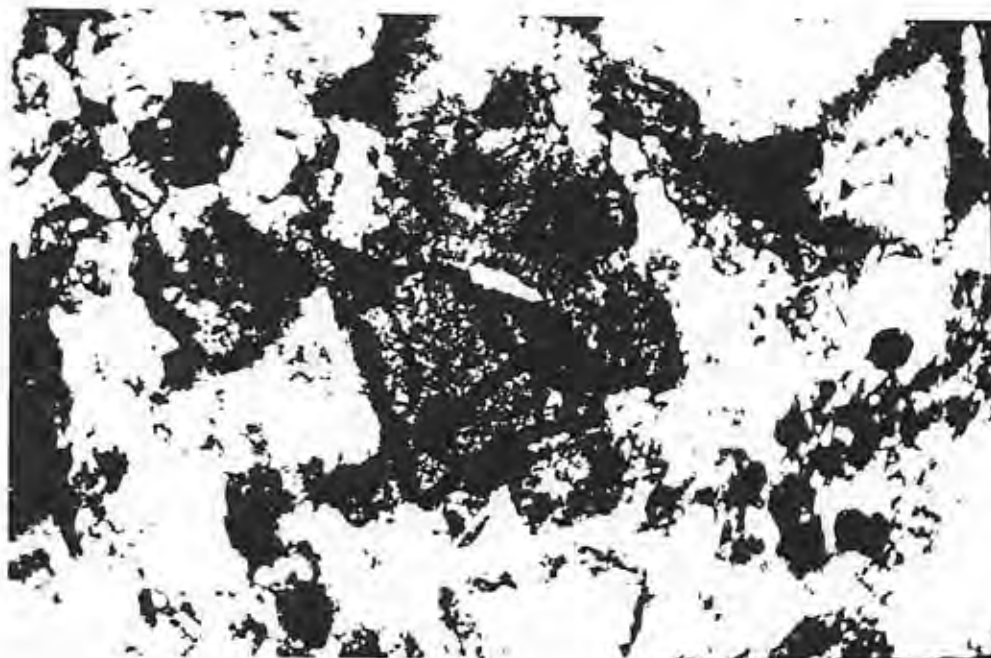


Figure 28. Photomicrograph of spinel in a highly fractured zone in red colored olivine (PPL, 2 mm across)

When viewed in reflected light, the main core of spinel shows a necklace of secondary anhedral spinels in a silicate rim along the circumference of the original spinel grain (Figure 29). There is a discrete silicate phase around the margin of the original main spinel grain, but composition for the spinel phase could not be determined using the available optical methods. This silicate is thought to be a discrete phase associated with an alteration or recrystallization of the original spinel. Thus, the necklace of secondary spinel surrounding the main spinel could be interpreted either as:

1. an exsolution effect of the individual spinels into an existing surrounding silicate,
2. a breakdown assemblage of amphibole into feldspar and spinel in which the amphibole rimmed an original spinel grain or
3. growth features which formed as an Fe^{3+} -rich liquid precipitated a spinel phase around the original spinel

Microprobe analyses do not yet exist to determine subtle differences in primary or secondary compositions. The secondary rimmed spinel phase is anhedral in form and exist as a discrete phase which surrounds the main spinel. Necklace-like clusters of secondary spinels are



Figure 29. Photomicrograph of spinel with a necklace
-like growth around the grain
(Reflected light, approx 1 mm across)

often connected to each other suggesting larger original spinels. The primary spinels found in all three textural types of xenoliths are aluminum-rich and consequently do not appear entirely opaque between crossed nicols.

Summary and discussion

The mineralogy within all the texturally distinct types of xenoliths is found to be very similar. Texturally, there are at least two distinct types of xenoliths seen (Type G* and Type C). The silicate phases present in the rock indicate that the depth of origin is deep crustal or upper mantle. Thermobarometric analysis (next chapter) supports this interpretation and minimum depths of 45 kilometers are inferred. Thus some interpretations could be made regarding the origin of the different xenolith types.

One possibility is that the original rock has been deformed to varying degrees because of differential pressures in the upper mantle (or the location of crystallization). This would result in the different textures seen, but cannot explain the cause of xenoliths being colored.

A second possibility is that each xenolith type has formed in a different location under varying degrees of hydrostatic pressure. This accounts for a variation in

grain size.

Reheating of green colored xenoliths in a variety of environments failed to produce a red color, but discoloration of the initial emerald-green to a brownish color is seen. Preliminary room temperature infrared analyses suggest that changes are taking place within the xenoliths.

The visibly red colored samples predominantly have Type G* textures. The red coloring is believed to be caused as a result of oxidation of the ferrous ion in the original olivine structure. In the Toroweap Valley features, the olivines exhibit fingers of the red phase growing laterally into the host mineral, olivine (Figure 26). In many cases, the fingers penetrate through the entire grain. Perpendicular to these fingers, secondary fingers can be seen (Figure 27). The composition of the red phase was not identifiable in petrologic thin section, but is believed to be a hematite phase similar to that described in Haggerty et al (1967). The spinel phase in the red xenoliths appears to decompose and diffusion from the breakdown may result in the discoloration of phases other than the olivine. The enstatite grain in the red xenolith appear deep brown in color.

GEO THERMOMETRY AND GEOBAROMETRY

Introduction

Using the theoretical single pyroxene thermobarometer of Mercier (1980), pyroxene geothermometry and geobarometry (hereafter termed thermobarometry, after Mercier) were attempted to evaluate the pressure and temperature of crystallization of the mantle peridotite xenoliths. This author wrote a computer program in GW-BASIC (see Appendices II and III) for IBM and compatible personal computers based on programs written previously by Mercier (1980) in FORTRAN and by Weiss (1983) in BASIC.

The purpose of this method was to (a) test the validity of the textural classification scheme developed by this author for xenoliths found in the Toroweap Valley, by estimating the pressure-temperature environment of crystallization of the xenoliths, (b) to test the thermobarometer by applying it to the Toroweap Valley samples and (c) to evaluate the results relative to the tectonics of the region.

Method of analysis

Electron microprobe analysis was performed on samples of all three textural types from five localities (shown in

Figure 4) from the Toroweap Valley, and the relevant results were used in the thermobarometer. Data from four localities on Vulcan's Throne were also used (B. Hanson, pers. comm) as were data from the three textural types defined by Best (1974).

Electron Microprobe sample preparation

Samples from the three textural types of peridotite xenoliths from the Toroweap Valley were crushed, and individual grains <30 mesh and >60 mesh were hand picked under a binocular microscope. There was a very common occurrence of poikilitically enclosed spinels and care was taken to select phase-pure minerals for analysis. The samples were then mounted in a multihole bakelite disk and a clear casting resin was carefully poured in the individual holes taking care to avoid formation of air bubbles. After curing in air for at least eight hours, the hardened disks were then hand polished using successively finer polishing powders and finally using 0.5 micron Al_2O_3 powder for a final polish. The disks were ultrasonically cleaned between successive polishing powders to prevent uneven polishing and plucking. Careful polishing is necessary to remove as much surface topography from the individual minerals to prevent defocussing during microprobe analysis.

Electron Microprobe analysis

Electron microprobe analysis was undertaken at Pennsylvania State University, University Park, Pennsylvania under the guidance of Mr. Lee Eminghizer. An ETEC microprobe was used with an accelerating voltage of 15 kilovolts and a specimen current of 0.02 microamps. The computer-interlocked microprobe was operated using interactive software and an Albee-Ray correction program. The accuracy of the instrument is within 2% of the amounts reported. The Fe content is reported as total FeO. The reader is referred to Brozdowski (1983), for example, for an extensive description of the machine and its operation. For a theoretical outlook on the microprobe technique the reader is referred to Hutchinson (1974).

Clinopyroxene and orthopyroxene grains from five locations in the Toroweap Valley were examined. These represented the three texturally defined varieties described earlier (previous section). Data from Vulcan's Throne and from localities in the Western Grand Canyon region (Hanson, pers. comm.; Best, 1974) were also used to compare with the data from the Toroweap Valley.

The cation proportions in the pyroxenes were applied to a theoretical pyroxene thermobarometer and the results compared with the Basin and Range geotherm.

Theory and limits of the thermobarometer

Many workers (Davis and Boyd, 1966; Boyd, 1973; MacGregor, 1974; Presnall, 1976; Herzberg, 1978) have theoretically and experimentally determined, from the pressures and temperatures of crystallization of mineral aggregates, that the solubility of Al_2O_3 in orthopyroxene varies as a function of pressure. The Al_2O_3 isopleths, when plotted as a function of pressure and temperature are sufficiently steep to be used as a geobarometer (MacGregor, 1974). However, there is considerable debate over the slope of the lines obtained (MacGregor, 1974; Presnall, 1976) and thus the validity of the Al_2O_3 geobarometer is therefore in question. For this study the Al_2O_3 isopleths are assumed steep enough to be used as a geobarometer.

Boyd (1973) used the $\text{Ca}/(\text{Ca} + \text{Mg})$ ratio in kimberlites from South Africa as a geothermometer and this geothermometer has proved useful in estimating the depth of formation of many coexisting minerals and has been cross-checked widely with other estimates of the continental geotherm.

The Mercier thermobarometer used in this study makes certain basic assumptions, all of which may not be truly applicable to the naturally occurring mineral aggregates.

Nevertheless, application of this thermobarometer to similar rocks worldwide have provided useable results. The first assumption is that one pyroxene phase (clinopyroxene or orthopyroxene) coexisted with at least one other pyroxene and an aluminum-rich phase (spinel or garnet). This assumption is made to calculate pressures of crystallization based on Al_2O_3 solubility. Most other geobarometers use data from two coexisting pyroxenes; this one simplifies the model by assuming coexistence of the phases.

The second assumption is that the pyroxenes analyzed could be resolved into endmember phases of the diopside and enstatite solid solution. This assumption is used for temperature estimation wherein the clinopyroxene and the orthopyroxene are used to determine the $Ca/(Ca+Mg)$ ratio for pyroxene.

The third and certainly the most questionable assumption is that the system with pure endmembers is free of iron in the lattice structure.

The thermobarometer used in this study is developed using a thermodynamic approach and is derived from the classical pressure equation:

$$P = (R.T.\ln K' + T.\Delta S - \Delta H) / \Delta V$$

where enthalpy (ΔH), entropy (ΔS) and changes in volume (ΔV) are obtained from experimental data and/or empirical models (Mercier, 1980). The partition coefficients K' , have been derived from many natural assemblages. Appendices II and III list the detail method of calculation used in this study. Mercier (1980) found that for the pressure-temperature range considered, the partition of Ca between enstatite and diopside is independent of pressure and strongly dependent on temperature, whereas Al is extremely sensitive to pressure changes while being relatively insensitive to temperature.

To compute the depth of origin of the coexisting phases, the relationship $km=3.04x+6$ where x is the calculated pressure in kbs. (Boyd, 1989). This relationship is based on the continental geotherm of Boyd (1983) and has been successfully applied to the Lesotho kimberlites.

Results

From thin section studies, the spinel and silicate phases in the xenolith samples from the Toroweap Valley were found to typically show a significant amount of deformation and alteration (see section on Petrography). This is seen characteristically in Type C xenoliths which show a significant deformation fabric. The

occurrence of unequivocal major amounts of garnet remained unconfirmed, but there was observed highly altered trace amounts of suspected garnet. Thus the thermobarometer used in this study was evaluated for pressures and temperatures in both the spinel as well as the garnet stability fields. Accordingly, the results from microprobe analysis of single pyroxenes were applied assuming both stability fields and the results compared. Samples from the Toroweap Valley were analyzed and the results applied to the thermobarometer as were results from similar analyses on Vulcan's Throne samples (Best, 1974; this study).

Spinel-facies stability results

Table 4 lists the pressure-temperature-depth estimates for different pyroxenes which are plotted in P-T-space (Figure 30). The relative phase transitions and geotherms that are used for relative comparison are obtained from various sources.

Different values were obtained from clinopyroxene (cpx) and orthopyroxene (opx) evaluation. In general the cpx (solid circles) yield higher pressure estimates than the opx (open circles). There is no definite relationship that can be seen with respect to the temperature variation. A characteristic difference seen within the

TOROWEAP VALLEY XENOLITHS

<u>SAMPLE</u>	<u>PcpX</u>	<u>TcpX</u>	<u>DcpX</u>	<u>PopX</u>	<u>TopX</u>	<u>DopX</u>
H3A				16.99	1010.04	57.65
				± 1.05	± 3.97	± 9.19
H3B	24.44	1027.41	80.30	18.43	1007.49	62.03
	± 0.20	± 1.83	± 6.60	± 0.97	± 2.89	± 8.95
H14A-1	22.09	979.96	73.15	18.09	965.66	60.99
	± 0.70	± 0.36	± 0.13			
H18A	22.338	977.3	73.90	22.53	943.91	74.49
				± 0.26	± 5.18	± 0.79
H20-1	20.37	984.21	67.92			
	± 2.24	± 11.22	± 12.81			
H25-3	21.88	996.23	72.51			
	.3=0.23	.3=2.0	.3=6.70			

BEST's XENOLITHS

<u>SAMPLE</u>	<u>PcpX</u>	<u>TcpX</u>	<u>DcpX</u>	<u>PopX</u>	<u>TopX</u>	<u>DopX</u>
E63	19.411	1003.869	65.01	15.919	1013.897	54.39
V85	17.74	927.136	59.92	14.42	952.95	49.84
			± 2.23	± 2.66	± 12.78	
V86	19.023	932.910	63.83	20.671	943.847	68.84

VULCAN's THROWE XENOLITHS

<u>SAMPLE</u>	<u>PcpX</u>	<u>TcpX</u>	<u>DcpX</u>	<u>PopX</u>	<u>TopX</u>	<u>DopX</u>
VTERD-1	19.579	1013.54	65.52	17.476	1026.067	59.13
	.3=0.15	.3=1.76	.3=6.46			
B24F				20.02	944.67	66.86
				± 1.24	± 22.85	± 9.77
VTLF6M				22.702	954.078	75.01
VITWP9-4	18.724	966.71	62.92	20.148	1008.652	67.25

P : Calculated pressure

T : Calculated temperature

D : Calculated depth; ($D = (P * 3.04) + 6$ (Boyd,1989))

Table 3

Average pressure, temperature and depth estimates
for pyroxenes assuming spinel-facies stability.

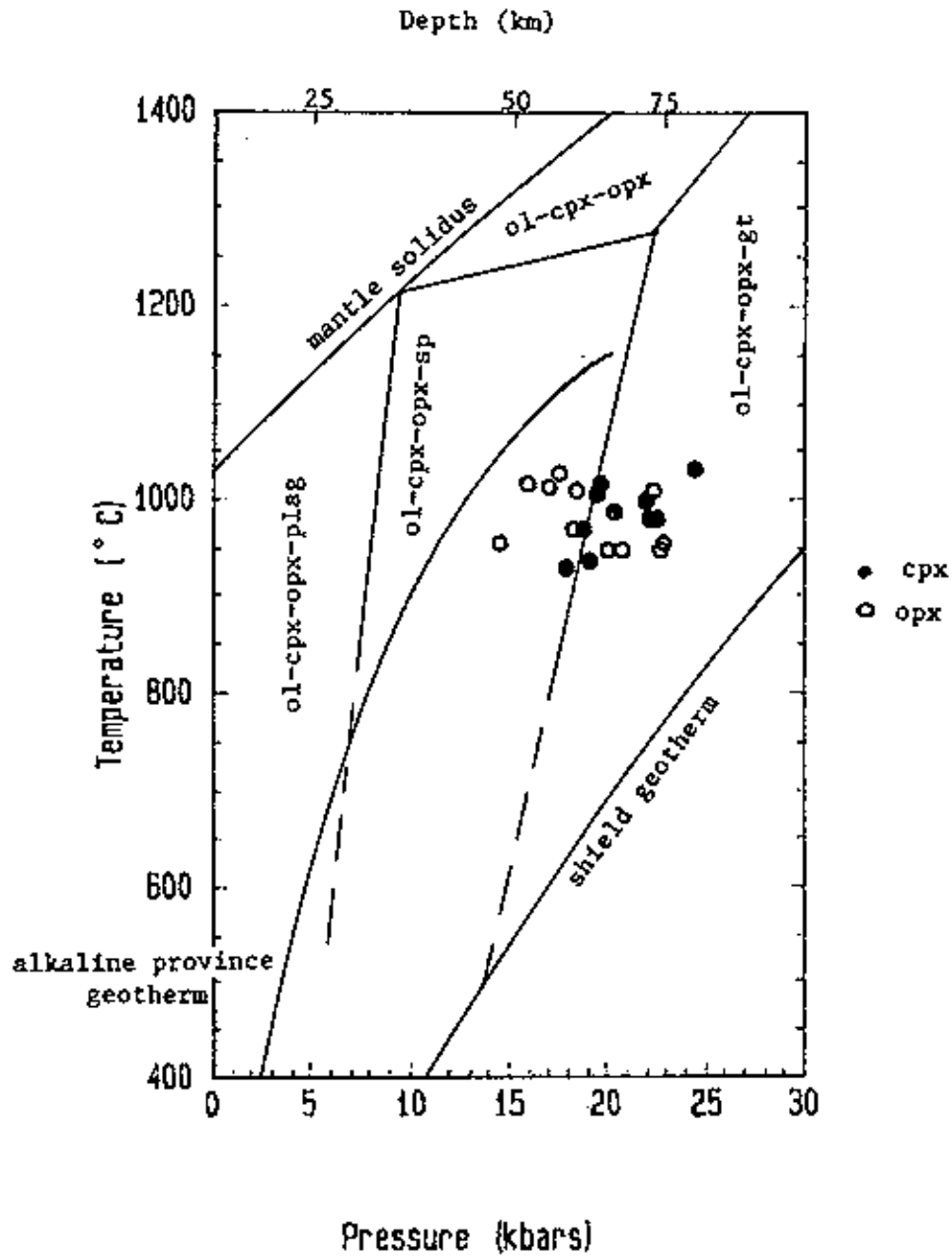


Figure 30 Plot of Pressure vs Temperature vs Depth for pyroxenes from different xenoliths in the Western Grand Canyon region, assuming spinel-facies stability

samples is that the Vulcan's Throne samples yield lower pressures than the Toroweap Valley samples. This also yields a shallower inferred depth of origin for the Vulcan's Throne and Best's (1974) xenoliths than the Toroweap Valley xenoliths. The Toroweap Valley samples all lie within the garnet stability field whereas the samples from Vulcan's Throne lie either in the spinel stability field or on the experimentally determined garnet-spinel phase boundary.

This calculation is made assuming that the xenolith assemblage formed in the spinel peridotite stability field (olivine + clinopyroxene + orthopyroxene + spinel) and that garnet is absent. Classical geophysical models of the interior of the earth (Ringwood, 1975) suggest that the maximum depth to which the spinel phase is stable for the samples studied here ranges between 60.7km (18kb) and 66.8km (20kb) (Figure 30). However, the minimum depth estimated for the Toroweap Valley features is 57km (16.9 kb), and 59.1km (17.5kb) for the Vulcan's Throne xenoliths. All the points lie between the inferred alkaline province geotherm and the shield geotherm, and tend to lie closer to the former.

Petrographic analysis (Best, 1974; this study) suggests that garnet may be present, in either a highly altered state or in trace amounts. Thus the thermobarometer is

applied with parameters for both the spinel and garnet stability fields and the results compared.

Garnet-facies stability results

The garnet facies results, on the other hand yield lower pressures and higher temperatures as compared with the spinel facies results (Figure 31 and Table 5).

Assuming garnet stability of the phase assemblage (olivine(ol) + clinopyroxene(cpx) + orthopyroxene(opx) + garnet(gt)), the pressure and temperature evaluations yield a much larger scatter than is seen in the spinel model results. The cpx yields lower temperatures than the opx. This is characteristically different from the overlap seen using the spinel facies model (see Figure 30). All but two clinopyroxene results and one orthopyroxene lie within the spinel stability field. The opx results cluster around the alkaline province geotherm. The pressure estimates are found to be generally lower than those determined in the spinel facies (compare Figures 30 and 31) and lie within the spinel stability field irrespective of the textural type of xenolith analyzed. Consequently, the depths estimated here are lower than in the spinel stability model. Minimum depths estimated are 52.9km (15.4kb) for xenoliths from the Toroweap Valley features, 45.7km (13kb) for

TOROWEAP VALLEY XENOLITHS

<u>SAMPLE</u>	<u>PcpX</u>	<u>TcpX</u>	<u>DcpX</u>	<u>PopX</u>	<u>TopX</u>	<u>DopX</u>
M3A				19.87	1132.42	66.40
				± 0.11	± 3.75	± 6.33
M3B	18.11	1115.21	61.05	18.51	1129.86	62.27
	± 0.92	± 3.2	± 8.80	± 0.44	± 4.43	± 7.38
H14A-1	19.17	971.72	64.28	15.752	1080.981	53.89
	± 0.93	± 0.65	± 8.80			
H18A	25.959	968.099	84.92	19.44	1062.86	65.10
			± 0.98	± 5.21	± 8.98	
H20-1	16.69	975.85	56.74	15.440	1058.758	52.94
	± 0.250	± 12.21	± 6.76			
H25-3	17.54	988.48	59.32			
	.3=0.26	.3=1.76	.3=6.79			

BEST'S XENOLITHS (1974)

<u>SAMPLE</u>	<u>PcpX</u>	<u>TcpX</u>	<u>DcpX</u>	<u>PopX</u>	<u>TopX</u>	<u>DopX</u>
E63	13.082	991.417	45.77	13.153	1132.022	45.99
V85	14.713	912.688	50.73	13.56	1061.34	47.22
			± 0.84	± 0.36	± 8.55	
V86	15.626	919.498	53.50	16.178	1060.467	55.18

VULCAN'S THROWE XENOLITHS

<u>SAMPLE</u>	<u>PcpX</u>	<u>TcpX</u>	<u>DcpX</u>	<u>PopX</u>	<u>TopX</u>	<u>DopX</u>
VTERD-1	14.32	1008.80	49.53	17.294	1149.774	58.57
	.3=0.35	.3=1.92	.3=7.06			
VTERD-1	14.804	1006.609	51.00			
B24F				21.98	1059.77	72.82
				± 0.83	± 24.64	± 8.52
VTLF6H				16.759	1074.506	56.95
VITNF9-4	15.671	958.514	53.64	20.385	1133.786	67.97

P : Calculated pressure

T : Calculated temperature

D : Calculated depth; ($D = (P \cdot 3.04) + 6$ (Boyd, 1989))

Table 4

Average pressure, temperature and depth estimates
for pyroxenes assuming garnet-facies stability.

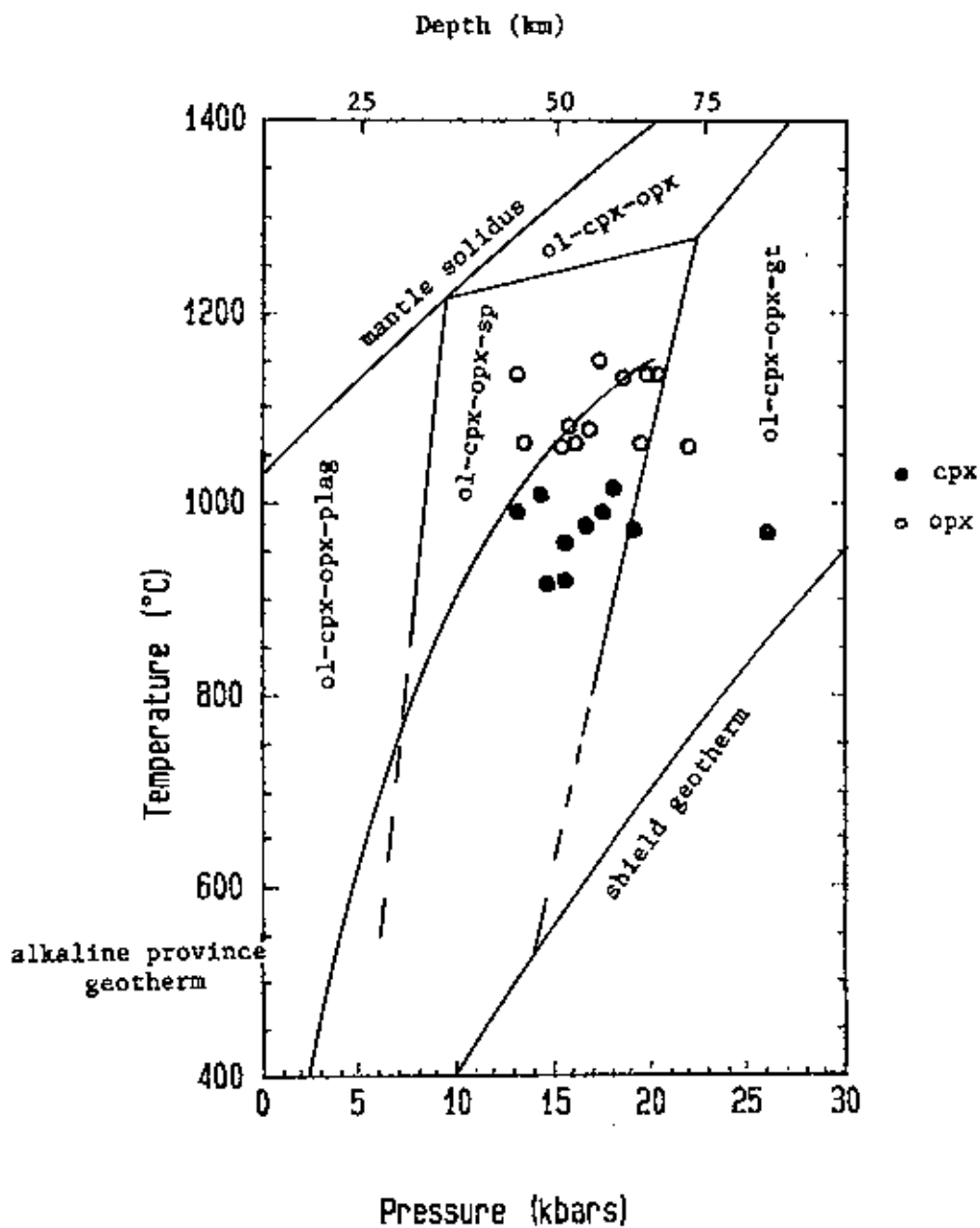


Figure 31. Plot of Pressure vs Temperature vs Depth for pyroxenes from xenoliths from different Western Grand Canyon locations assuming garnet facies stability

Best's (1974) analyses 49.5km (14.3kb) for the Vulcan's Throne xenoliths.

Discussion

To address the first aim of this exercise, namely to try to distinguish source areas between the different textural varieties of xenoliths defined, it is found that this cannot be done with any certainty. On the other hand, if the Toroweap Valley samples and the Vulcan's Throne samples are compared regardless of the thermobarometer used, the latter yield significantly lower pressure estimates. This fact does indicate that the pressure environment was less by at least 3-4 kilobars. This would translate to being a difference of at least 10 kilometers in depth between the xenolith source area for the two localities. This appears consistent with the textural differences seen between samples from the two areas. The Vulcan's Throne samples and those described by Best (1974) show a grain size that is larger by a factor of at least 2. A higher pressure could probably imply or allow a larger grain size, but if high pressure is also coupled with deformation, as is evidenced by the Toroweap Valley xenolith fabrics seen, this grain size reduction may be the result more of deformation than total lithostatic pressure during crystallization of the mantle.

In general estimates of the pressure and temperature of the xenolith source region have been achieved using the Mercier thermobarometer, and if the depth equivalent of the pressure/temperature is introduced, it is indicative that the minimum calculated depth of crystallization of the xenoliths in the Vulcan's Throne-Toroweap Valley area is at least 45 kms. The pressure-temperature estimate is also found to be significantly higher than the alkaline province geotherm. Since the xenolith samples are found in fundamentally alkaline lavas, the fact that the xenoliths do not lie very near the aforementioned geotherm is significant. The other point that bears importance is the tectonic location of the study area. It is believed to be a part of the Colorado Plateau by some workers (Best, 1970; Hamblin, 1972; Fenniman, 1932), the Basin and Range by others (Brumbaugh, 1987) and a transition zone between the two by yet another group (Best and Brimhall, 1974). The crustal thickness of the Basin and Range province is believed to be in the order of 20 kilometers whereas that of the Colorado Plateau is at least 40 kms. The minimum depth of crystallization inferred from the thermobarometer indicates that the study area is either in a transition zone or belongs to the Colorado Plateau for the xenoliths to have originated in the upper mantle.

The third aim is to evaluate the validity of the

thermobarometer relative to the Toroweap Valley samples. It is seen that different pressure-temperature estimates are obtained when different pyroxenes are considered; different results are obtained when spinel stability and garnet stability are assumed. What is peculiar is that when spinel stability is assumed, the results from the theoretical thermobarometer yield P-T estimates that lie within the garnet stability field (Figure 31) whereas if one assumes garnet stability for the original phase, the thermobarometer yields P-T estimates that lie both within the spinel stability field and the garnet stability field (Figures 30 & 31). This implies that the thermobarometer cannot be successfully applied to the Toroweap Valley samples, and interpretation must be made with extreme caution. Nevertheless, the relative pressures and temperatures, when compared within each stability field (sp and gt), show sufficient variation to suggest a greater depth of origin for the Toroweap Valley samples than Vulcan's Throne.

The final aim is to evaluate the results obtained above relative to the tectonics of the region. As discussed earlier, the results indicate that the xenoliths originate in a Basin and Range-Colorado Plateau transition zone between the Basin and Range province and the Colorado Plateau. This is consistent with the geophysical evidence

of the study area (Brumbaugh, 1987). Physiographically (Fenniman, 1932), the Western margin of the Colorado Plateau incorporates the study area. The pressure-temperature-depth estimates, coupled with the fact that fundamentally alkaline volcanism occurs in the Toroweap Valley and vicinity indicates that the region is located in a tectonically more active region. Age dating (Best and Brimhall, 1974) of the Toroweap lavas yield eruption times of 2-4 million years ago. It is believed that rifting still occurs today and that the Basin and Range margin is migrating eastward into the Colorado Plateau. The minimum depths of origin of the peridotite xenoliths suggest a rather thick crust overlying the mantle (≤ 40 kms). The crustal thickness of the Basin and Range has been estimated as being to the order of 20 kms (Baldridge et. al., 1989) and that of the Colorado Plateau being at least 40 kms. This, coupled with the structured nature of the region suggests that the Toroweap Valley area is located in a transition zone between the Basin and Range-Colorado Plateau which supports the model proposed by Hamblin and Best (1980), and thus this author believes that the region lies within a transition zone that resembles more the Basin and Range province than the Colorado Plateau.

CONCLUSIONS

This study yields a number of interesting results that help in understanding the geologic history of the southern edge of the Toroweap Valley. The conclusions that are made from this study can be listed as follows:

1) The basanite features found in the Toroweap valley can be interpreted as mantle-vent features that have erupted from upper mantle depth.

2) A comparative chemical analysis shows compositional differences that exist between the samples from the features in the Toroweap Valley, the lavas on Vulcan's Throne and the Uinkaret lava flows. The basanite features and the average flow composition are found to have a more primitive origin than Vulcan's Throne even though they erupted at a later date.

3) A model proposed by this author suggests that the basanite features and the basanite lava flows originate from the same magma chamber whereas the lava flows from Vulcan's Throne originate from a magma chamber at intermediate depth. This intermediate chamber derives its magma

from the parental magma chamber.

4) Three different textural types of peridotite xenoliths are found within the Toroweap Valley. This implies that at least three environments existed in the magma chamber as, or following the crystallization of the xenoliths. The textures seen in xenoliths from the Toroweap Valley are similar, but cannot be classified using the system developed by Best (1974) for xenoliths in the Western Grand Canyon region.

5) Pressure-temperature calculations suggest a depth of origin of at least 45 kilometers for Vulcan's Throne xenoliths and at least 53 kilometers for the Toroweap Valley samples, thus indicating a distinct source region for each location. These estimates support geophysical evidence that the Toroweap Valley lies in a transition zone between the Basin and Range and Colorado Plateau Provinces, as suggested by some studies. An important factor that must be considered is that the geothermobarometer used in this study can be applied only in a relative sense to the Toroweap Valley xenoliths because of the wide scatter of results that are obtained.

6) The unique red colored xenoliths found scattered

throughout the Toroweap Valley features and on Vulcan's Throne are believed to be caused as a result of reheating of originally green colored peridotite xenoliths. This reheating causes an alteration within the olivine grains, which show a deep-red phase, visible in thin section, penetrating the entire mineral. This phase is believed to be either hematite or laihunite, or a combination of the two ferric-rich phases that is precipitated along crystal planes and defects within the mineral as a result of reheating of the xenoliths at depth. The spinel phase in the red xenoliths, also seen to decompose, probably contributes to the red coloring that is seen.

REFERENCES

- Atwater T (1970) Implications of plate tectonics for the Cenozoic tectonic evolution of western North America. Geol. Soc. America Bull., v. 81, 3513-3536.
- Baldrige WS and Olsen KB (1989) The Rio Grande rift. Am. Sci., v. 77: 240-247.
- Best MG (1970) Kaersutite-Peridotite Inclusions and Kindred Megacrysts in Basanitic Lavas, Grand Canyon, Arizona. Contrib Mineral Petrol. v.27:25-44.
- Best MG (1974a) Mantle-derived amphibole within inclusions in alkalic-basaltic lavas. J. Geophys. Res. v.79:2107-2113.
- Best MG (1974b) Contrasting types of Chromium-Spinel Peridotite Xenoliths in Basanitic Lavas, Western Grand Canyon, Arizona. Earth Planet Sci. Lett. v.23:229-237.
- Best MG (1975) Amphibole Bearing cumulate inclusions Grand Canyon, Arizona, and their bearing on silica-undersaturated hydrous magmas in the upper mantle. J. Petrol. v.16:212-236.

Best MG and Brimhall WH (1974) Late Cenozoic Alkalic Basaltic Magmas in the Western Colorado Plateaus and the Basin and Range Transition Zone USA, and their bearing on Mantle Dynamics. Geol. Soc. Amer. Bull. v.85:1677-1690.

Boyd FR (1973) A pyroxene geotherm. Geochim. Cosmochim. Acta v.37:2533-2546.

Breed WJ and Roat ED, editors (1974) Geology of the Grand Canyon. c. N. Ariz. Soc., Sci. ART, Inc. Mus. of North. Ariz. and Grand Canyon Nat. Hist. Assoc., publishers.

Brozdowski (1983) Geologic Setting and Xenoliths of the Lodge Pole intrusive area: implications for the northern extent of the Stillwater complex, Montana. U.S.A. MA Thesis, Temple University.

Brumbaugh DS (1987) A tectonic boundary for the southern Colorado Plateau. Tectonophysics. v.136:125-136.

Carter JL (1977) Comparison of ultramafic and mafic xenoliths from Kilbourne Hole and Potorillo Maar, New

- Mexico. Second Int. Kimberlite Conf., Santa Fe
(extended abstracts, unpagged).
- Christiansen RL and Lipman PW (1972) Cenozoic volcanism
and plate-tectonic evolution of the Western United
States. II.-Late Cenozoic. Phil. Trans. R. Soc. Lond.
A. v271:249-284.
- Clark SP, Jr. (1966) Handbook of Physical constants.
Geological Society of America Memorial 97.
- Davis BTC and Boyd FR (1966) The join $Mg_2Si_2O_6$ -
 $CaMgSi_2O_6$ at 30 Kilobars pressure and its applications
to pyroxenes from kimberlites. J. Geophys. Res.
v.71:3567-3576.
- Fenniman (1932) *Physiography of the Western U.S.*
- Gary M, McAfee R, Jr. Wolf CL, editors (1972) Glossary of
Geology. Amer. Geol. Inst. Washington, D.C.
- Ginsburg IV, Lisitsina GA, Sadidova AT, Sidorenko GA
(1962) Fayalite of Granite rocks and the products of
its alteration (Kuraminskii Range, Central Asia), Akad.
Namk. CCCP, Trudy Mineralog. Museya v.13: 16-42 (in

Russian)

Griffin WL and O'Reilly SY (1987) The composition of the lower crust and the nature of the continental Moho - xenolith evidence. in Mantle Xenoliths, P.H. Nixon, editor (1987).

Haggerty SE and Baker I (1967) The Alteration of Olivine in Basaltic and Associated Lavas. Part I: High Temperature Alteration. Cont. Mineral. and Petrol. v.16:233-257.

Hamblin WK (1974) Late Cenozoic Volcanism in the Western Grand Canyon. Geology of the Grand Canyon, Breed WJ and Roat EC, editors Northern Arizona Soc. Sci. Art, Inc.

Hamblin WK and Best MG, Editors (1970) Guidebook to the Geology of Utah, No. 23 The Western Grand Canyon District. Utah Geolog. and Mineral. Survey. Univ. Utah, Salt Lake City, Utah.

Herzberg CT and Chapman NA (1976) Clinopyroxene geothermometry of spinel lherzolites. Am. Min. v.61:626-637.

Hutchinson CS (1974) X-ray Fluorescence Spectrometry. From Laboratory Handbook of Petrographic Techniques. John Wiley and Sons, Inc. New York, pp. 264-281.

Laihunite Research Group, Guiyang Institute of Geochemistry, Academia Sinica, and 101 Geological Team of Lianing Metallurgical and Geological Prospecting Company (1976) Laihunite - a new iron silicate mineral, *Geochemica* 6:95-103 (in Chinese)

Laihunite Research Group, Institute of Geochemistry, Academia Sinica, and Geological Team No. 101 of Lianing Metallurgical and Geological Prospecting Company (1982) Laihunite - a new iron silicate mineral, *Geochemistry* 1:105-114.

Leavy BD and Hermes OD (1979) Mantle xenoliths from southeastern New England. In Boyd FR and Meyer HOA editors, *The mantle sample: inclusions in kimberlites and other volcanics.* (Proc. Intl. Kimberlite Conf. No.2 v.2) 424pp American Geophysical Union, Washington, D.C.

MacGregor ID (1974) The system $MgO-Al_2O_3-SiO_2$:

Solubility of Al₂O₃ in enstatite for spinel and garnet periodotite compositions. Am. Mineral. v.59:110-119.

Matson D et. al. (1984) Volatiles in amphibole from xenoliths, Vulcan's Throne, Grand Canyon, Arizona, U.S.A. Geochim. et Cosmochim. Acta v.48:1629-1636.

Mercier (1980) Single Pyroxene Thermobarometry. Tectonophysics v.77:1-37.

Pike and Schwarzman (1977) Classification of Textures in Ultramafic xenoliths. Jour. Geol. v.85:49-61.

Presnell DC (1976) Alumina content of enstatite as a geobarometer for plagioclase and spinel lherzolites. The American Mineralogist v.61:582

Ringwood AE (1975) Composition and Petrology of the Earth's Mantle McGraw Hill, Publishers.

Ryan MP and Blevins JYK (1987) Viscosity of Synthetic and Natural Silicate Melts and Glasses at High Temps and 1 Bar (10⁵ Pascals) pressure and at higher pressures. USGS Bull 1764.

- Schaefer MW (1983) Crystal chemistry of Ferric-rich fayalites. PhD Thesis, Mass. Inst. Tech.
- Weiss DS (1984) A Study of the Petrography, Phase Chemistry, Volatile Inclusions and Intrinsic Oxygen Fugacity of Composite Group II Ultramafic Xenoliths from San Carlos, Arizona. Masters Thesis, Temple Univ., PA.
- Yoder HS, Jr. (1969) Contemporaneous Rhyolite and basalt. Carnegie Inst. Year Book 69, No. 1580:141-145.

APPENDIX I

Computer program in GWBASIC to
calculate the settling velocity
of a xenolith in a mobile lava.

```

10 PRINT "PROGRAM TO COMPUTE SETTLING VELOCITY OF A SAMPLE IN A MOBILE MEDIUM U
SING STOKES LAW AND THE LAWS OF MOTION"
30 REM THE DENSITY OF THE SAMPLE AND THE FLOW ARE FIXED
50 PRINT "AUTHOR: LINUS FARIAS, TEMPLE UNIV., DEPT OF GEOLOGY, PHILA, PA 19121.
1989 ":PRINT:PRINT
70 PRINT "TITLE ": INPUT TIT$
90 PRINT TIT$:PRINT
110 INPUT "ENTER THE BODY DIAGONAL OF THE SAMPLE IN CMS ": DIA: PRINT
130 RAD = (DIA/2)
150 INPUT "ENTER THE VISCOSITY OF THE MEDIUM IN POISES ": VIS: PRINT
170 INPUT "ENTER THE DENSITY OF THE SAMPLE": D1
190 INPUT "ENTER THE DENSITY OF THE MEDIUM": D2
210 DEN = (D1 - D2)
230 RAD2 = (RAD * RAD)
250 VEL = (2 * RAD2 * DEN * 978.072)/(9 * VIS)
270 VEL1 = (VEL * 3600)/100
290 PRINT :PRINT "THE SETTLING VELOCITY OF THE SAMPLE IN A STATIC FLOW IS ": VEL
:" cm/s OR ": VEL1:"m/hr": PRINT
310 INPUT "ENTER THE THICKNESS OF THE FLOW IN METERS ": H
330 HCM = H * 100
350 T = (2 * HCM)/VEL
370 TMIN = T/60
390 PRINT: PRINT " THE TIME TAKEN FOR THE XENOLITH TO SETTLE IN A FLOW ": H; "ME
TERS THICK IS ": T; " SECONDS OR": TMIN; "MINUTES":PRINT
410 INPUT "ENTER THE VELOCITY OF THE FLOW IN METERS PER HOUR ":VFLO: PRINT
430 DIST = VFLO * (TMIN/60)
450 PRINT " THE DISTANCE THE XENOLITH WILL TRAVEL BEFORE IS REACHES THE BASE OF
THE FLOW IS ": DIST; " METERS"
470 INPUT "DO YOU WANT A PRINTOUT ":PRT$
490 IF PRT$ ="Y" GOTO 510 ELSE 530
510 LPRINT "FOR THE SAMPLE": TIT$: " WITH BODY DIAGONAL ": DIA; " cm AND VISCOI
TY OF THE MEDIUM ": VIS; " poises, THE DISTANCE TRAVELLED WILL BE ": DIST; " MET
ERS AND THE TIME THAT IT WILL TAKE FOR THE XENOLITH TO SETTLE IS ": TMIN; " MINU
TES"
530 INPUT "DO YOU WANT ANOTHER RUN ": ANS$
550 IF ANS$ = "Y" GOTO 70
570 END

```

APPENDIX II

Computer program in GWBASIC to calculate
the pressure and temperature of pyroxenes
using the Mercier (1980) thermobarometer
assuming spinel-facies stability.

```

90  REM  MERCIER CPX GEOTHERM, GEOBAROM, SPINEL FACIES
110 REM PROGRAM WRITTEN BY LINUS FARIAS, 1/1989
130 IF (ENDIS = "D" OR ENDIS = "d") THEN P1= 419.76:P2= 616.61:D1= 11.2724:D
21= 32.371:T1= -7537.5:T2= 61152!
150 DS = CHR$ (4)
170 PRINT "MERCIER SINGLE PYROXENE THERMOBAROMETRY: TECTONOPHYSICS, V. 42 PP 1-
36, 1980. SPINEL FACIES"; PRINT DS
180 LPRINT "MERCIER SINGLE PYROXENE THERMOBAROMETRY: TECTONOPHYSICS, V. 42 PP 1
-36, 1980. SPINEL FACIES"
190 GOTO 230
210 CLS
230 REM ENTER SAMPLE ID
250 INPUT "SAMPLE ID= ";PYX$:PRINT PYX$:LPRINT DS "SAMPLE ID= ";PYX$:LPRINT
270 REM ENTER AS ENSTATITE OR DIOPSIDE
290 INPUT "ENTER IF SAMPLE IS EN or DIOP (E or D ONLY) ";ENDIS:PRINT ENDIS
310 IF (ENDIS = "E" OR ENDIS = "e") THEN P1= 351.32:P2= 299.13:D1= 8.675101:
D2= 24.568:T1= -6308.5:T2= 45449!
330 IF (ENDIS = "D" OR ENDIS = "d") THEN P1= 419.76:P2= 616.61:D1= 11.2724:D
21= 32.371:T1= -7537.5:T2= 61152!
350 REM ENTER CATIONS PER 6 OXYGEN
370 GOSUB 770
390 REM CALCULATE OR NORMALISED
410 GOSUB 1030
430 REM CALCULATE THE W AND KW VALUES
450 GOSUB 1110
470 REM CALCULATE THE A, KS AND KA VALUES
490 GOSUB 1230
510 REM CALCULATE D
530 GOSUB 1390
550 REM CALCULATE NUMP
570 GOSUB 1490
590 REM CALCULATE NUMT
610 GOSUB 1590
630 REM CALCULATE PRESSURE
650 GOSUB 1690
670 REM CALCULATE TEMPERATURE
690 GOSUB 1790
710 INPUT "MORE RUNS (Y or N) "; ANS$
730 LPRINT:LPRINT:LPRINT
750 IF ANS$ = "Y" GOTO 210 ELSE GOTO 1950
770 REM LIST CATIONS
790 PRINT "ENTER THE FOLLOWING CATIONS PER 6 OXYGENS":PRINT DS
810 INPUT "SI= ";SI: PRINT DS:PRINT SI:LPRINT "SI= ";SI: PRINT DS
830 INPUT "TI= ";TI: PRINT DS:PRINT TI:LPRINT "TI= ";TI: PRINT DS
850 INPUT "AL= ";AL: PRINT DS:PRINT AL:LPRINT "AL= ";AL: PRINT DS

```

```

870 INPUT "FE= ";FE: PRINT D$:PRINT FE:LPRINT "FE= ";FE: PRINT D$
890 INPUT "MN= ";MN: PRINT D$:PRINT MN:LPRINT "MN= ";MN: PRINT D$
910 INPUT "MG= ";MG: PRINT D$:PRINT MG:LPRINT "MG= ";MG: PRINT D$
930 INPUT "CA= ";CA: PRINT D$:PRINT CA:LPRINT "CA= ";CA: PRINT D$
950 INPUT "NA= ";NA: PRINT D$:PRINT NA:LPRINT "NA= ";NA: PRINT D$
970 INPUT "CR= ";CR: PRINT D$:PRINT CR:LPRINT "CR= ";CR: PRINT D$
990 RETURN
1010 REM CHROME NORMALISED
1030 FCR! = CR/(AL + CR - NA)
1050 PRINT "CHROME NORMALISED FCR = ";FCR!
1070 LPRINT "CHROME NORMALISED FCR = ";FCR!
1090 RETURN
1110 REM COMPUTE W AND KW
1130 W! = CA/(CA + MG + FE + MN)
1150 IF (ENDIS="a" OR ENDIS="E") THEN KW! = (61 * W!)/(1-(2 * W!))
1170 IF (ENDIS="d" OR ENDIS="D") THEN KW! = (1 - (2*W!))/(.667 + (.667 * W!))
1190 LPRINT "KW"= ";KW!": PRINT "W = ";W!
1210 RETURN
1230 REM CALCULATE A, KS AND KA VALUE
1250 A! = (AL - NA)/2
1270 IF (ENDIS="a" OR ENDIS="E") THEN KAD! = (1 - (2.87 * (FCR!)))^2
1290 IF (ENDIS="d" OR ENDIS="D") THEN KAD! = (1 - (1.27 * (FCR!)))^2
1310 KA! = A!/(1-A!)/KAD!
1330 LPRINT "A= ";A!, KAD!, "KA"= ";KA!
1350 PRINT "A= ";A!, KAD!, "KA"= ";KA!
1370 RETURN
1390 REM CALCULATE D
1410 D! = (LOG(KA!) * LOG(KW!)) - (D1! * LOG(KW!)) + (2.2595 * LOG(KA!)) + D2!
1430 PRINT "THE VALUE OF THE DENOMINATOR D IS: ";D!
1450 LPRINT "THE VALUE OF THE DENOMINATOR D IS: ";D!
1470 RETURN
1490 REM CALCULATE NUMP
1510 NUMP! = (P1! * LOG(KW!)) - (706.14 * LOG (KA!)) + P2!
1530 PRINT "THE NUMERATOR FOR PRESS CALCN IS: ";NUMP!
1550 LPRINT "THE NUMERATOR FOR THE PRESSURE CALCN IS: ";NUMP!
1570 RETURN
1590 REM CALCULATE NUMT
1610 NUMT! = (T1! * LOG(KW!)) + T2!
1630 PRINT "THE NUMERATOR FOR TEMP CALCN IS: ";NUMT!
1650 LPRINT "THE NUMERATOR FOR THE TEMPERATURE CALCN IS: ";NUMT!
1670 RETURN
1690 REM CALCULATE P
1710 P! = NUMP!/D!
1730 PRINT "THE THEORETICAL PRESSURE IS ";P!;" KILOBARS"
1750 LPRINT "THE THEORETICAL PRESSURE IS ";P!;" KILOBARS"
1770 RETURN
1790 REM CALCULATE T
1810 T! = NUMT!/D!
1830 T1! = T! - 273.15
1850 PRINT "THE THEORETICAL TEMPERATURE IS ";T!;" DEG KELVIN"
1870 PRINT "THE THEORETICAL TEMPERATURE IN DEGREES C IS ";T1!
1890 LPRINT "THE THEORETICAL TEMPERATURE IS ";T!;" DEGREES KELVIN"
1910 LPRINT "THE THEORETICAL TEMPERATURE IN DEGREES C IS ";T1!
1930 RETURN
1950 END

```

APPENDIX III

Computer program in GWBASIC to calculate
the pressure and temperature of pyroxenes
using the Mercier (1980) thermobarometer
assuming garnet-facies stability.

```

90  REM MERCIER CPX GEOTHERM, GEOBAROM, GARNET FACIES
110 REM PROGRAM WRITTEN BY LINUS FARIAS, 2/1989
130 REM PROGRAM REWRITTEN FROM FORTRAN.
150 D$ = CHR$(4)
170 PRINT "MERCIER SINGLE PYROXENE THERMOBAROMETRY: TECTONOPHYSICS, V. 42 PP 1-
36, 1980.  GARNET FACIES": PRINT D$
180 LPRINT "MERCIER SINGLE PYROXENE THERMOBAROMETRY: TECTONOPHYSICS, V. 42 PP 1
-36, 1980.  GARNET FACIES"
190 GOTO 230
210 CLS
230 REM ENTER SAMPLE ID
250 INPUT "SAMPLE ID= ";PYX$:PRINT PYX$:LPRINT D$ "SAMPLE ID= ";PYX$:LPRINT
270 REM ENTER AS ENSTATITE OR DIOPSIDE
290 INPUT "ENTER IF SAMPLE IS EN or DIOP (E or D ONLY) ";ENDI$:PRINT ENDI$
310 IF (ENDI$ = "E" OR ENDI$ = "e") THEN P1! = 176.43:P2! = -264.9:D1! = 6.2079:D2
! = 31.037:T1! = -3168.1:T2! = 53754!
330 IF (ENDI$ = "D" OR ENDI$ = "d") THEN P1! = 176.43:P2! = -224.56:D1! = 6.901:D2
! = 29.471:T1! = -3168.1:T2! = 53754!
350 REM ENTER CATIONS PER 6 OXYGEN
370 GOSUB 790
390 REM CALCULATE CR NORMALISED
410 GOSUB 1050
450 REM CALCULATE THE W AND KW VALUES
470 GOSUB 1130
490 REM CALCULATE THE A, KAD AND KA VALUES
510 GOSUB 1250
530 REM CALCULATE D
550 GOSUB 1390
570 REM CALCULATE MUMP
590 GOSUB 1490
610 REM CALCULATE NUMT
630 GOSUB 1590
650 REM CALCULATE PRESSURE
670 GOSUB 1690
690 REM CALCULATE TEMPERATURE
710 GOSUB 1790
730 INPUT "MORE RUNS (Y or N) "; ANS$
750 LPRINT:LPRINT:LPRINT
770 IF ANS$ = "Y" GOTO 210 ELSE GOTO 1950
790 REM LIST CATIONS
810 PRINT "ENTER THE FOLLOWING CATIONS PER 6 OXYGENS":PRINT D$
830 INPUT "SI= ";SI: PRINT D$:PRINT SI:LPRINT "SI= ";SI: PRINT D$
850 INPUT "TI= ";TI: PRINT D$:PRINT TI:LPRINT "TI= ";TI: PRINT D$
870 INPUT "AL= ";AL: PRINT D$:PRINT AL:LPRINT "AL= ";AL: PRINT D$
890 INPUT "FE= ";FE: PRINT D$:PRINT FE:LPRINT "FE= ";FE: PRINT D$

```

```

910 INPUT "MN= ";MN: PRINT D$:PRINT MN:LPRINT "MN= ";MN: PRINT D$
930 INPUT "MG= ";MG: PRINT D$:PRINT MG:LPRINT "MG= ";MG: PRINT D$
950 INPUT "CA= ";CA: PRINT D$:PRINT CA:LPRINT "CA= ";CA: PRINT D$
970 INPUT "NA= ";NA: PRINT D$:PRINT NA:LPRINT "NA= ";NA: PRINT D$
990 INPUT "CR= ";CR: PRINT D$:PRINT CR:LPRINT "CR= ";CR: PRINT D$
1010 RETURN
1030 REM CHROME NORMALISED
1050 IF (ENDIS= "E" OR ENDIS= "e") THEN FCR! = CR/(AL + CR - NA)
1060 IF (ENDIS= "D" OR ENDIS= "d") THEN FCR! = CR/(AL + CR - (.57 * NA))
1070 PRINT "CHROME NORMALISED FCR = ";FCR!
1090 LPRINT "CHROME NORMALISED FCR = ";FCR!
1110 RETURN
1130 REM COMPUTE W AND KW
1150 IF (ENDIS= "E" OR ENDIS= "e") THEN W! = CA/(CA + MG + FE + MN)
1160 IF (ENDIS= "D" OR ENDIS= "d") THEN W! = CA/(CA + MG + FE + MN - (.18 * NA))
1170 IF (ENDIS= "E" OR ENDIS= "e") THEN KW! = (11.976 * W!)/(1-(2 * W!))
1190 IF (ENDIS= "D" OR ENDIS= "d") THEN KW! = (1 - (2 * W!))/(.833 + (.334 * W!))
1200 PRINT "KW" = ";KW! : PRINT "W = ";W!
1210 LPRINT "KW" = ";KW! : PRINT "W = ";W!
1230 RETURN
1250 REM CALCULATE A, KAD AND KA VALUE
1270 IF (ENDIS= "E" OR ENDIS= "e") THEN A! = (AL - NA)/2
1280 IF (ENDIS= "D" OR ENDIS= "d") THEN A! = (AL - (.57 * NA))/2
1290 IF (ENDIS="E" OR ENDIS="e") THEN KAD!=(1 - (.69 * (FCR!)))^2:KAN! = (A * (1 - A)) * (6.004 - (3.025 * MG) - (.702 * LOG(KW!)))
1310 IF (ENDIS="D" OR ENDIS="d") THEN KAD!=(1 - (.71 * (FCR!)))^2:KAN! = (A * (1 - A)) * (3.298 - (1.781 * MG) - (.128 * LOG(KW!)))
1330 KAI= KAN!KAD!
1350 LPRINT "A= ";A!, "KAN = ";KAN!, "KAD" = ";KAD!, "KA" = ";KAI
1370 RETURN
1390 REM CALCULATE D
1410 D! = (LOG(KAI) * LOG(KW!)) - (D1 * LOG(KW!)) + (2.2595 * LOG(KAI)) + D2!
1430 PRINT "THE VALUE OF THE DENOMINATOR D IS: ";D!
1450 LPRINT "THE VALUE OF THE DENOMINATOR D IS: ";D!
1470 RETURN
1490 REM CALCULATE NUMP
1510 NUMP! = (P1 * LOG(KW!)) - (706.14 * LOG(KAI)) + P2!
1530 PRINT "THE NUMERATOR FOR PRESS CALCN IS: ";NUMP!
1550 LPRINT "THE NUMERATOR FOR THE PRESSURE CALCN IS: ";NUMP!
1570 RETURN
1590 REM CALCULATE NUMT
1610 NUMT! = (T1 * LOG(KW!)) + T2!
1630 PRINT "THE NUMERATOR FOR TEMP CALCN IS: ";NUMT!

1650 LPRINT "THE NUMERATOR FOR THE TEMPERATURE CALCN IS: ";NUMT!
1670 RETURN
1690 REM CALCULATE P
1710 P! = NUMP!/D!
1730 PRINT "THE THEORETICAL PRESSURE IS ";P!;" KILOBARS"
1750 LPRINT "THE THEORETICAL PRESSURE IS ";P!;" KILOBARS"
1770 RETURN
1790 REM CALCULATE T
1810 T! = NUMT!/D!
1830 T1! = T! - 273.15
1850 PRINT "THE THEORETICAL TEMPERATURE IS ";T1!;" DEG KELVIN"
1870 PRINT "THE THEORETICAL TEMPERATURE IN DEGREES C IS ";T1!
1890 LPRINT "THE THEORETICAL TEMPERATURE IS ";T1!;" DEGREES KELVIN"
1910 LPRINT "THE THEORETICAL TEMPERATURE IN DEGREES C IS ";T1!
1930 RETURN
1950 END

```